POLITECNICO DI TORINO

Degree Course in Mechatronic Engineering

Master of Science Thesis

ENERGY MANAGEMENT TECHNIQUES FOR REGENERATIVE ACTIVE SHOCK ABSORBERS

Supervisors
Prof. Marcello Chiaberge

Candidate
Rosa Aurora Tenerelli

October 2018

to Marco, who believes in me more than I do.

CONTENTS

List of Figures

List of Tables

ABSTRACT

During any travel, vehicles present movements along their vertical axes due to road roughness, curved trajectory, braking, acceleration and inertial forces. The ordinary task of shock absorbers is to absorb the vertical oscillations, providing comfort to the driver, always maintaining the vehicle stability.
In particular, the active ones offer the possibility to change the damping coefficient and the chassis lifting.

The present study analyzes regenerative hydraulic active shock absorbers, i.e. active shock absorbers able to recover the vibrational energy into electrical one, and focuses on the design of a device able to route the recovered energy from the four corners shock absorbers into a battery.

Exploiting the reversibility of brushless machines used for the lifting operation in active mode, the suspension movement generates a current, mostly characterized by a frequency component equal to the switching frequency of the brushless machine.

This type of current is not suitable for battery charging. Starting from the constraints relative to the battery, and the analysis of the power flow, a DC/DC buck converter (whose output is represented by the port connected to the battery) has been identified as a solution. In order to design a proper current control, the converter has been modelled according to the state space average method. Combing this feedback control with a feedforward one on the converter input voltage, the device is able to smooth enough the current in input to the battery and provide to upper limits the voltages, according to the automotive standard and the battery needs.

Acknowledgment

I'd like to thank everyone has supported me during the course of academic studies;
In particular Prof Marcello Chiaberge, my supervisor, who offered me the opportunity to be part of this project;
Dario Gandini who tutored me with patience and willingness;
all the members of the mechatronic laboratory who made this path easy and enjoyable;
my family and to my friends;
a special thank goes to my mum and my dad who have always sustained me and have made possible my academic achievements.

INTRODUCTION

Motivations

Mobility evolution cannot avoid including the reduction of fuel consumption and CO_2 emissions. Consequently, vehicles and components design is more and more concerned by the environmental impact and regulatory requirement necessary to limit the effects of an exponential development of the automotive sector (Tab.1).
Energy storage represents key passage for the electrification of vehicles power-train, that nowadays is the most adopted solution to reduce fuel consumption and emissions, beyond the ones used in engine motor control.

Euro X	Fuel	CO g/km	HC g/km	NOx g/km	PM g/km
I (Jan.1992-Jan.1993)	Gasoline	2.72	0.97(HC+NOx)		-
	Diesel				0.14
II (Jan.1996-Jan.1997)	Gasoline	2.2	0.5(HC+NOx)		-
	Diesel	2	0.7(HC+NOx)		0.08
III (Jan.2000-Jan.2001)	Gasoline	2.3	0.2	0.15	-
	Diesel	0.64	0.56(HC+NOx)	0.5	0.05
IV (Jan.2005-Jan.2006)	Gasoline	1	0.1	0.08	-
	Diesel	0.5	0.3(HC+NOx)	0.25	0.025
V (Sep.2009-Jan.2011)	Gasoline	1	0.1	0.06	0.005*
	Diesel	0.5	0.23(HC+NOx)	0.18	0.005
VI (Sep.2014-Jan.2016)	Gasoline	1	0.1	0.06	0.005*
	Diesel	0.5	0.17(HC+NOx)	0.08	0.005

Table 1: The evolution over years of pollutant limits for automobiles. * Direct injection, lean mixture

Different structural areas of a vehicle are involved in dispersion of energy that could be otherwise recovered contributing to the observation of emission regulations. One of these areas is the suspension system (Fig 1) which has the double task of absorbing vibration effects due to road irregularities and providing comfort and safety for driver and passengers.

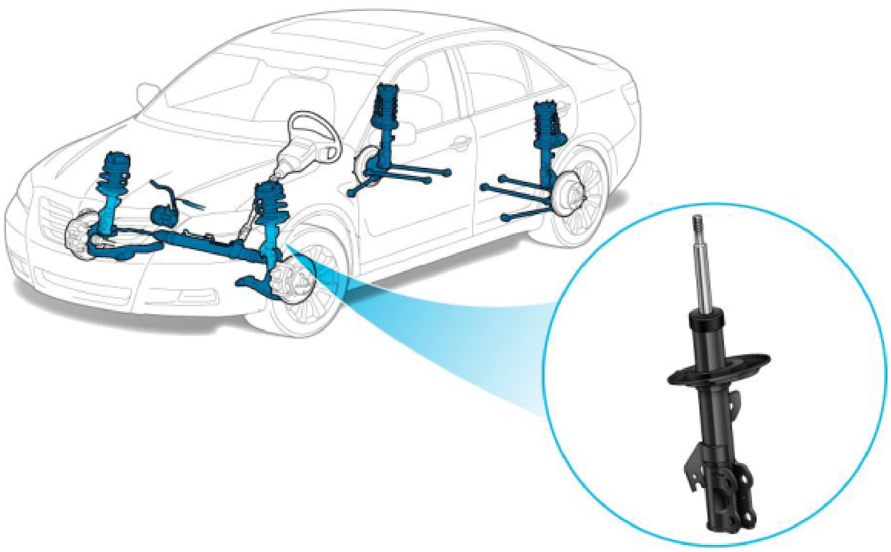

Figure 1: Suspension system.

Conventional suspensions are made up of a spring, a damper, and kinematic links, i.e. passive elements which manage the vibration effects mitigation by the conversion of mechanical energy into heat ([2]). It has been evaluated that the power dissipated in the form of heat by the four corner passive dampers is 133 W, for a car traveling at 32 km/h on a ISO C-class road profile. The recovery of the total amount of energy dissipated would mean a considerable emission reduction ([3]).

Objectives

The regenerative suspension system, which clearly has the additional task of energy recovery, recalls the idea of regenerative braking, diversifying itself for the employement of vibrational energy, instead of wheels kinetic one, for battery charging([4]).
The present study intends to analyze the hydraulic shock absorber model designed in [2] and [3], and considers it as a starting point for the development of a device able to properly charge a 48 V lead acid battery (Fig 2), assuming to have selected the optimal damping coefficient for the regeneration.

Battery charging methods have been object of a brief analysis in order to evaluate the worth of the obtained result. Since the hydraulic shock absorber has been modeled as a single one coupled to a battery, a further purpose has been to find a configuration that contemplate the four suspensions

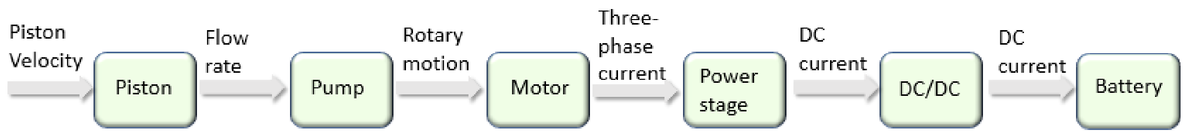

Figure 2: Power trasmission.

connection.
This means the four shock absorbers have to work simultaneously to charge a single battery. Clearly there is more than one way to connect the four corners together, in particular two of them have been identified and subjected to a selection.

Thesis organization

The thesis chapters are organized as follow:

State of art provides for:

- a brief overview about active shock absorber;
- examination of different ways in which regenerative active shock absorbers have been developed in literature;
- battery charging method overview and presentation of previous work in which the topic of battery charging by means of recovered power is dealt with.

Hydraulic regenerative active shock absorber:

- the method to realize a regenerative shock absorber designed by the mechatronic laboratory of the Polytechnic University of Turin is presented in detail. Since it represents the preparatory work and the background for this thesis study, it has been chosen to dedicate to it a chapter apart for a more detailed description.

Energy management:

- The recovered (acording to the model designed in [2]) current is analyzed in order to verify the necessity of the presence of a DC/DC converter and a constraints list is drown up for the safeguarding of the brushless motor and the battery;
- Different converter controlling approaches are investigated along the chapter sections;

- The coexistence of the four shock absorbers is analyzed and a configuration in which the four of them can charge a single battery is identified;
- Results and operational configuration of the final design are showed.

Design validation:

- the converter design is simplified and implemented by means of a multipurpose power module in order to provide for a test verification of the control strategy and the high view behavior of the coupling between the inverter-motor group and the converter.

Conclusion:

- the chapter provides for a summary of the thesis work, an overall efficiency analysis taking into account the entire shock absorber model, and a description of possible future application.

Chapter 1

State of Art

Vehicles are provided with a suspension system that, beyond holding the chassis, isolates the vehicle from road irregularities, limiting the vertical acceleration of the suspended mass, in order to improve the driving comfort.
Many vehicles employ passive shock absorbers, that are the simplest and the cheapest ones, hence the most used in commercial vehicles. They are essentially constituted by the parallel of a spring and a viscous damper, whose parameters are fixed and chosen as a trade of between driving comfort needs and handling requirements.
In fact, too soft suspensions improve comfort, since they rapidly deform compensating road asperities, but risking to reduce roadholding because of wide vertical oscillations and the resulting fluctuations of the contacting force between the tire and the road.

Sport cars have very hard suspensions, suitable for vehicle handling and roadholding but useless in everyday life. Passive shock absorbers performances are limited by the simplicity of the actuation devices and by the insufficient number of degree of freedom. For this reason, semi-active and active suspensions are more and more employed especially for sport or high cost cars.

Semi active shock absorbers are anyway made up of a spring-damper parallel system but also of a controlled actuator able to suitably vary the damping constant.

In active shock absorbers, beyond the spring and the damper is also present an actuator able to generate an internal time variable force between the vehicle chassis and the tire.
These systems, by means of an appropriate force modulation, let to stabilizing the movement obtaining higher performances with repect to passive suspensions.

A recent trend involves the use of electronic command circuits for the conversion of the dissipated energy into electrical one, increasing the overall efficiency system. In the last decade, many studies have been concerned the development of regenerative active shock absorbers, analyzing the different methods for the conversion of the mechanical vibration energy into electricity. Regenerative shock absorbers can be linear or interested by the linear to rotary motion conversion achieved by means of mechanical and/or hydraulic systems.
In Fig.1.1 are showed typical damper configurations that are strictly related to the layout of the vehicle suspension.

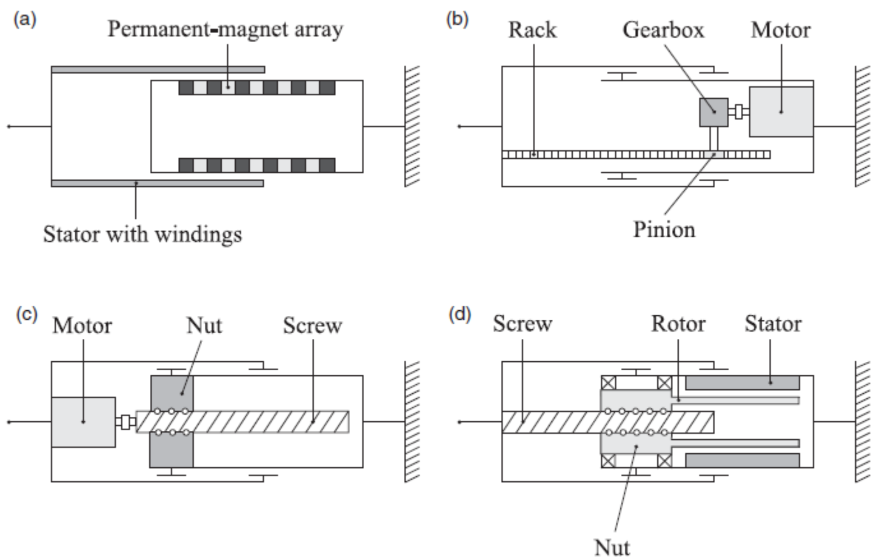

Figure 1.1: Possible configurations of the electromechanical shock absorbers (EMSA). (a) Linear, (b) rack–pinion, (c) ball screw, rotating-screw and (d) ball screw, rotating-nut([9]).

1.1 Regenerative active shock absorbers

1.1.1 Linear regenerative electromagnetic shock absorber

In [5], the working principle of regenerative electromagnetic shock absorber has been examined: exploiting the relative displacement between coils group and permanent magnet assembly, it behaves like a linear generator and provides damping actions.

The regenerative electromagnetic shock absorber is made up of four elements:

- a permanent magnet array

- a coil windings array
- two guide cylinders
- spiral spring

The permanent magnet array is tied to the vehicle wheel shaft and the coil windings array is connected to the vehicle body. When the vehicle drives on, the relative motion between vehicle body and wheel shaft generates a damping force opposite to the coil assembly.
The perpendicular movement of the conductor with respect to the magnetic field to identify the Lorentz force which induced an electromotive force and an eddy current in the coil cross section: hence power is recovered.
According to the paper, the shock absorber is feasible and actually provide for a regeneration current, though no reference about the current typology, as well as the battery charging, are present.

1.1.2 Regenerative active shock absorber exploiting electric motors

The rack pinion mechanism, employed for linear to rotary conversion, allows the usage of an electric rotary motor for the generator.
In a recent work ([6]), in order to increase the efficiency, the electric machine has been supplied with unidirectional angular motion, differently from conventional rotational regenerative shock absorbers in which mechanical vibration are converted into bidirectional rotation. The unidirectional motion is obtained by means of a clutch system.
Regenerative shock absorbers have been designed to be compact: a pair of rack and pinion, one shaft and three bevel gears have been used.
Two roller clutches connect the pinion with two larger bevel gears located at the opposite side of a third smaller bevel gear. At each movement direction of the pinion corresponds only one of the two larger bevel gears rotation: the large bevel gears rotates in opposite direction and are set on the two opposite sides of the small bevel gears, that thus, will always be driven in the same direction as well as the electric machine.
Pinion, shaft, and bevel gears have been mounted on a cylinder, while another cylinder is in charge to guiding the linear motion. The rotational motion transmitted to the DC generator make it to produce a back electromotive voltage proportional to the rotational speed.
The output recovered electrical powers has been measured on a load resistance, thus also in this study there is no mention to how this power could be actually employed for the charging of a battery.

A closer attention to the output power, recovered by a shock absorber that exploit the rack pinion mechanism, is given in [7]: although the power output has still been measured on an external resistance a power stage has been set up as output of the DC generator.

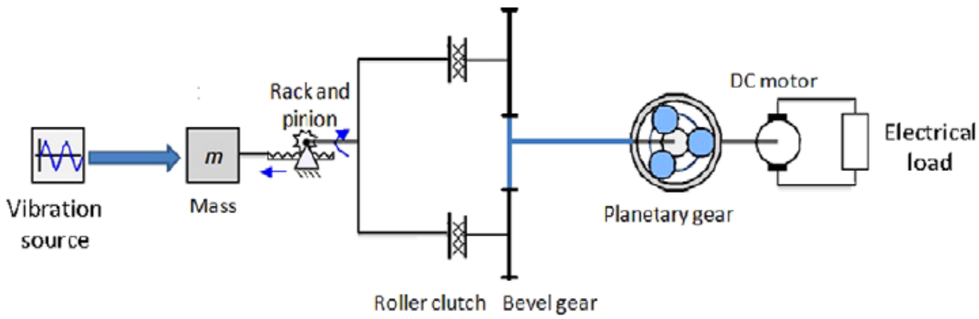

Figure 1.2: Simplified schematic view of the shock absorber with mechanical motion rectifier designed in [6]

The three- phase current generated by the brushless machine is unwitting and unsteady, thus not suitable for battery charging. A rectifier is needed, to convert the alternating three-phase current into a pulse-shape current, as well as a voltage regulator, used for providing power stability to loads.
Pulse-shape current is still no suitable for battery charging but does not cause issue for the chargin of super capacitor. Hence a super capacitor has been selected, rather than a battery, has been selected to store the electric recovered energy.

The ball screw mechanism is also common for linear to rotary motion conversion, coupled with an electric motor.
In work [8] the electro-mechanical actuator is constituted by DC motor and the ball screw mechanism, so that both, active suspension functionality and energy regeneration can be achieved. The linear vibration motion is converted into the motor input torque by means of the rotating screw.
Active suspensions provide damping control and, with it, energy saving, in fact the amount of energy recovered depends on the damping of the suspension system.

The ball screw mechanism has been also used in [9], with the difference that in this case is the nut, rather than the screw, to rotate. The overall structure of the regenerative shock absorber presented by the paper is described below: the motion, due to vibration, makes two concentric housing cylinders sliding.
The external cylinder holds the screw. A three-phase permanent-magnet brushless, whose rotor shaft is fixed to the nut, is the electric rotary machine placed in the internal cylinder.

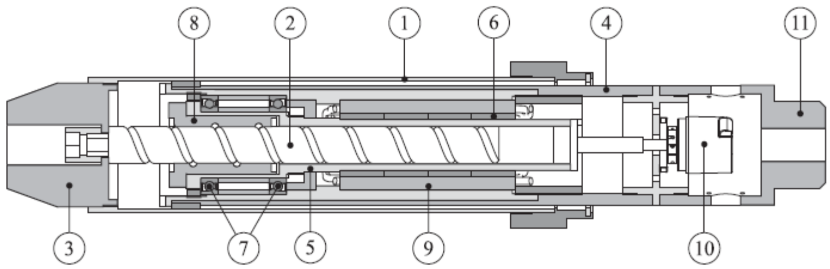

Figure 1.3: Shock absorber detailed section view. (1) Outer housing, (2) screw, (3) bottom cap, (4) inner housing, (5) rotor, (6) permanent magnets, (7) ball bearings, (8) nut, (9) stator, (10) encoder, (11) top cap. [9]

1.2 Battery charging

Traditionally there are two methods of charging lead-acid batteries (Fig.1.4)([?]):

- constant current charging
- constant voltage charging

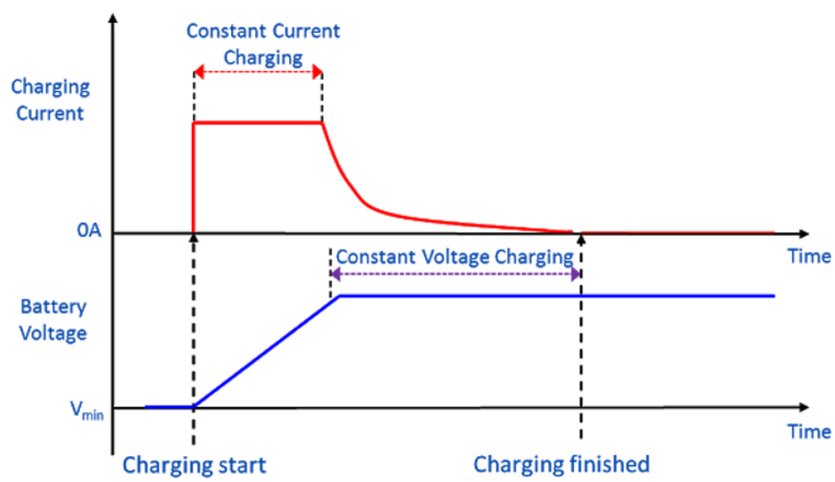

Figure 1.4: Comparison between constant current charging method and constant voltage charging method.

In the constant current charging method, the charger output voltage varies so that the current supplied to the battery could be uniform regardless of its state of charge. This charging method is suitable for batteries used in cycling application and requires that the charger removal when the battery is fully charged.

The preferred method for charging batteries in standby use is constant voltage charging method: the same voltage is applied to the battery, regardless state of charge (SOC). When the charging starts, the recharging current is high because of the high potential difference between the discharged battery and the charger, then, it gradually decreases as the battery voltage and SOC increases.
The constant voltage charging provides for two common charging voltage levels: float and equalize. In the former case the battery is recharged and maintained in a fully charged condition by keeping the battery at a voltage level that will maintain its charge. Instead, in the equalize or boost charging, the charger voltage level is higher than the float charge voltage in order to obtain a quicker recharge.

The literature explores the topic of designing a regenerative shock absorber fully, but it's often lacking in the analysis of the way in which the recovered power could actually charge a battery.

The regenerative hydraulic shock absorber presented in [11] is very similar to the one designed in [2] except from the fact that the motion rectification takes place after the transition trough the generator rather than before. Overlooking the shock absorber hydro-mechanical part, that will be fully explained in the following chapter, the electrical system is made up of the generator, a rectifier circuit, a DC voltage step up circuit, a diode and finally the battery.
The study analyzes the battery perspective focusing on different states of charge but always considering a constant angular velocity of the generator, i.e. a very unlikely situation.

Although in [11] had been also designed the circuit that make possible the battery charging, no explanation about components choices nor about control strategies are given.
In order to find work that present more complete analysis about the recovered energy management, it' necessary to broaden the research field. Renewable energy sources papers generally pay specific attention to the charging circuit.

In [12] study, the purpose is to charge more battery sets each connected to a microgrid by means of DC/DC and DC/AC converters.
The DC/DC controller consists in local voltage and current loops implemented through a proportional-integral (PI) controller (Fig.1.5); an extra State of Charge loop, based on an average-based control, has been added so that the overall control object is not only the traditional voltage and current control, but also the equalizing of the SoC of all battery sets (i.e. the average of all SoC values could be equal to that of each SoC).
The SoC of each battery set is measured, and in the decentralized controller of the DC/DC inverter

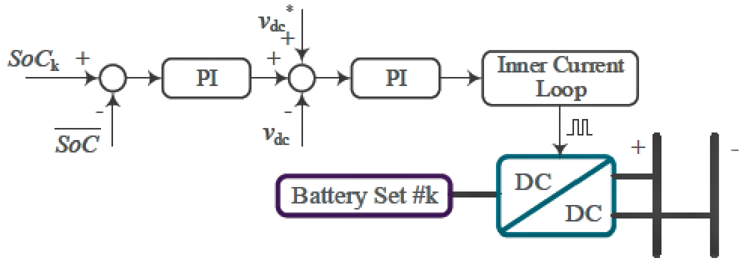

Figure 1.5: Conventional DC voltage and current control loop ([12]).

their average is computed.
Considering the dynamics of SoC as a slow one, the average-based loop has been designed as the outer loop, thus its output is provided to the inner voltage and current cascaded control loops as an additive term.
The work shows remarkable differences with the situation analyzed in the present thesis, such as the source of recovered energy and the number of battery, anyway the control strategy developed could be properly modified suitably for the purpose of storing the energy recovered by the active shock absorber in a battery.

In [13], a DCDC buck converter was built, and its controller was developed (Fig. 1.6), for battery chargers because of its application in many applications including renewable energy sources, inverters, electric vehicles and robots. The work offers a detailed description of the converter modeling as well as of the controller synthesis: the buck characteristic transfer function has been obtained by means of the state space averaging modeling, while the controller is composed by two nested loops, an internal peak current mode controller, and an external voltage controller.
The controller is designed so that the converter output voltage follows the given reference. The voltage controller produces current command signal to the peak current control loop.
The designed control system shows good results but, they obtained feeding the converter with a constant voltage. Once more the general structure represents a hint for the achieving of this thesis purpose, but is still far from its conclusion.

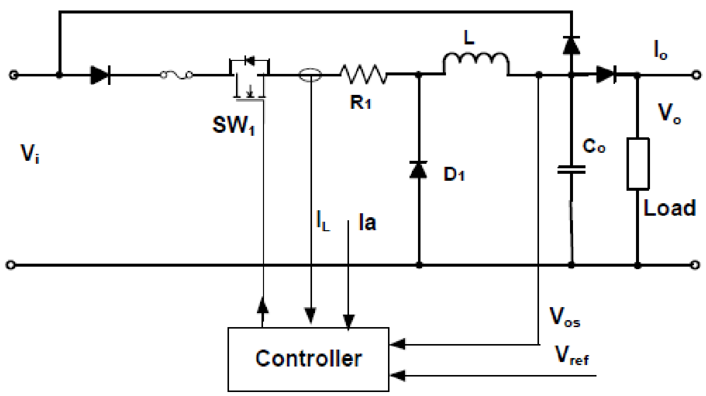

Figure 1.6: The developed DC-DC buck converter control system (1.6).

CHAPTER 2

PREPARATORY WORK: REGENERATIVE HYDRAULIC ACTIVE SHOCK ABSORBERS

The present study deals with the funneling of the energy coming from the active shock absorbers in the 48 V battery charging. Hence it requires, as starting point, the analysis and comprehension of the regenerative suspension model (Fig.2.1) and its control.

In the mechatronic laboratory of the Polytechnic University of Turin and Magneti Marelli Shock

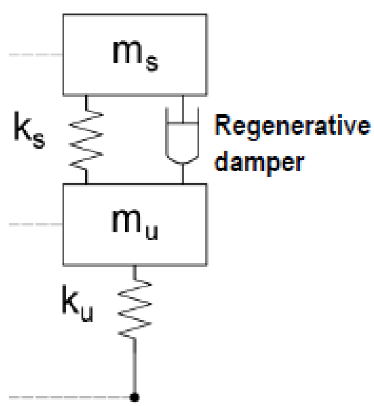

Figure 2.1: Quarter car model: m_s sprung mass, m_u unsprung mass, k_s suspension stiffness, k_u tire stiffness.

Absorbers, in the context of a research contract, an electro-hydrostatic version of the regenerative shock absorbers has been designed.
This solution has been preferred to the others previously presented,since it is a compromise among work efficiency, force density value, integration simplicity, fatigue resistance and actuator placement

flexibility.
The reference vehicle for the model development is the Jeep Renegade (Fig.2.2). *All the chapter is a*

Figure 2.2: Jeep Renegade.

brief explenation of [2]

2.1 Design

In suspension framework it's necessary a system able to convert linear motor into angular displacement because of the presence of a rotary electric motor. These systems are usually based on mechanical (rack pinion, ball screw) or hydraulic working principle.

Although electromechanical technologies present positive aspects, they are difficult to integrate into the suspension, since component wear and fatigue are crucial issues, not yet fully clarified, to be taken into account in a vehicle damping task.

In order to obtain suspensions systems, able to harvest energy using controllable damping coefficient the electro-hydrostatic actuation principle has been exploited. Hydraulic shock absorbers (showed in Fig. 2.3) use a hydro-static circuit for the piston linear movement into a rotational one, thus the critical aspects of the electomechanical system are overcome by the usage of the fluid that, beyond being intrinsically lubricated, provides better flexibility as power transmission mean.

The hydraulic regenerative dampers ability of energy harvesting is greatly effected by the motor-pump unit, hence the integration of hydraulic, mechanical and electric subsystems have been optimize to get the maximum energy recovery without losing the damping feature and considering design constraints.

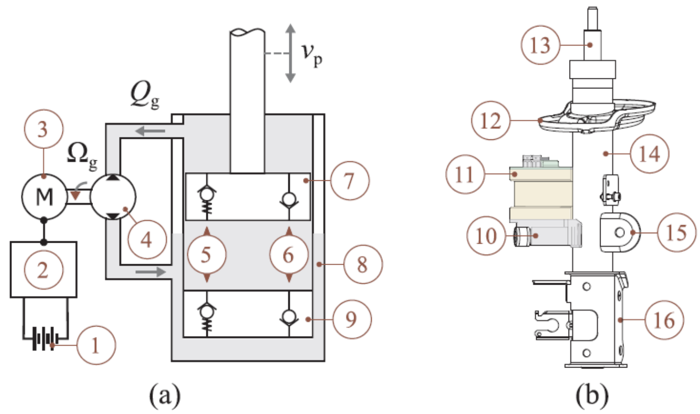

Figure 2.3: Layout of a hydraulic regenerative shock absorber([2]). Concept scheme (a): battery (1), power stage (2), electric motor (3), hydraulic pump (4), pressure-relief valves (5), check valves (6), piston (7), gas accumulator (8), base (9). Prototype side view (b): manifold (10), motor-pump unit (11), spring holder (12), rod (13), external tube (14), anti-roll bar bracket (15), wheel hub bracket (16).

A proper motor-pump design must deal with the different constraints concerning with the working domain of the shock absorber (Fig. 2.4). The damping specifications are used to define the pump geometric design, and together with the resulting device parameters, to set up the machine electromagnetic design.
From the DC supply voltage specifications, the turns number of the electrical machine windings has been obtained. The motor-pump design has been validated through thermal analysis.
The power stage components are choosen in order to be compliant with electric machine parameters and the supply requirements. The damping envelope and the physical limitations had been taken into account for the development of the control strategy.

2.2 Architecture

A gerotor pump has been employed for the development of the hydraulic active suspension.In fact, because of its fixed displacement, this device offers relevant advantages with respect to other hydraulic pumps (reduced tooth wear, low amount of components, fluid power system integration).

The system works employing a conventional twin-tube shock absorber architecture directly linked to the hydraulic pump ports. When the vehicle is moving, because of the ground irregularities, the shock absorber piston oscillates in the tube at a speed v_g. The oil flow rate Q_g caused by the piston

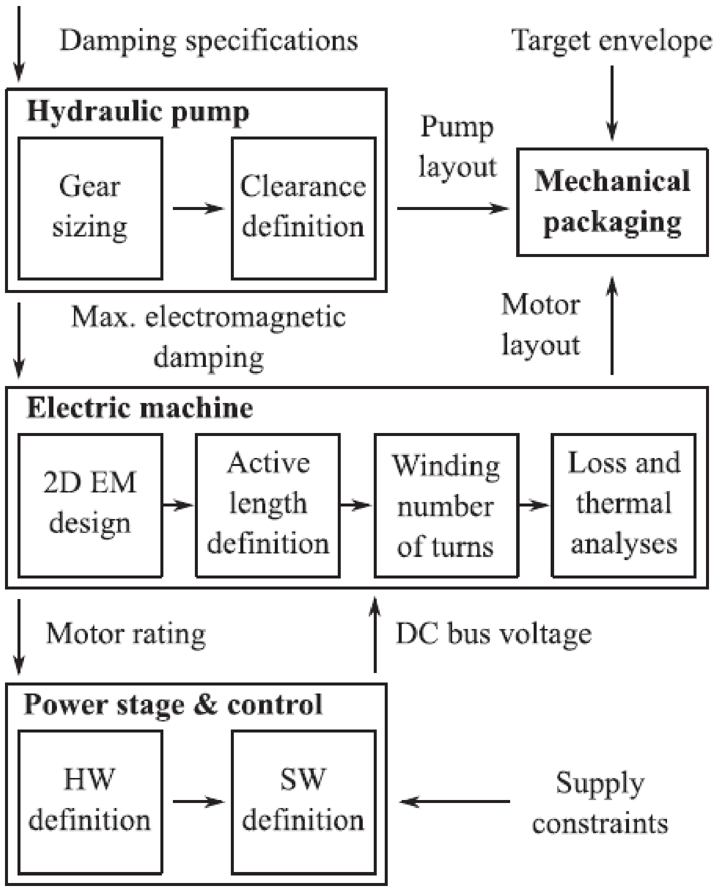

Figure 2.4: Design method for the motor-pump unit ([2])

motion drives the hydraulic pump, so that the linear movement is converted into a rotation Ω_g. The pump is mechanically coupled to a brush-less machine, which acts as a generator in a portion of the damping quadrants.
This architecture makes the system capable to provide electrical energy, for example to a battery, starting from the kinetic one generated by the suspension motion. As presented in previous works, [3], the twin-tube rectifies the fluid flow so that the motor-pump units are supplied with unidirectional motion. In order to minimize the hydraulic lines losses, and to provide a certain system modularity, a manifold is employed to integrate the motor-pump group into the shock absorber tube.

The electric machine was designed according to the damping constraints when in short circuit.
Since active power is not necessary to make the motor working within the damping specifications, a brushless permanent-magnet (PM) machine represent a solution for the torque-to-mass ratio maximization. In particular an inner rotor, radial flux, surface-mounted PM motor has been employed in

the shock absorber architecture.

The power stage is made up of s three-phase full bridge, so that the active mode work can be guaranteed. The bridge employs three MOSFET phase legs chose according to the motor rating.

Field oriented control strategy is used (Fig. 2.5). It consists in a PI compensator whose sampling

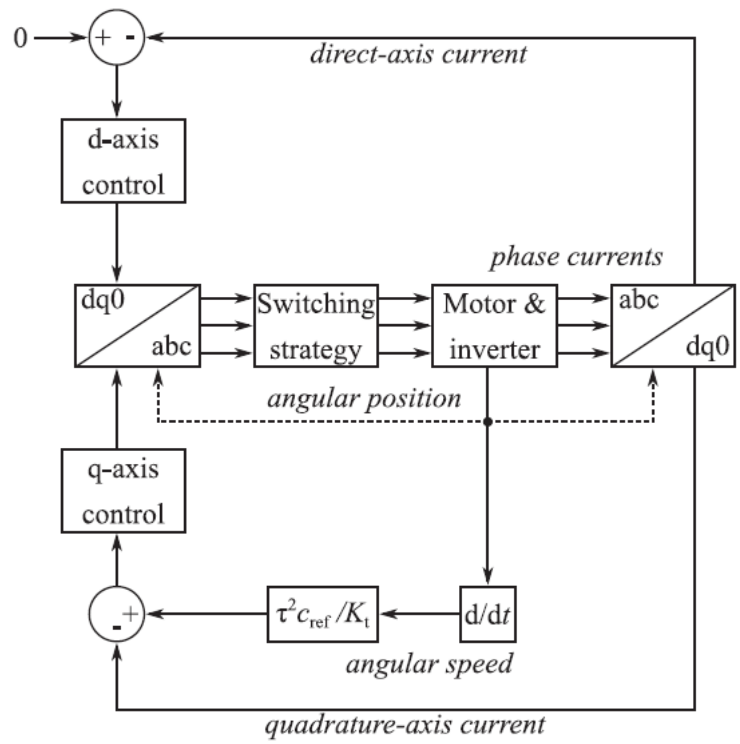

Figure 2.5: Block diagram of the control strategy for the motor-pump unit. ([2])

frequency is equal to the phase switching one. Since the brushless machine control concerns only the constant-torque region, the direct current reference is assumed equal to zero; the quadrature current instead is obtained by means of a reference damping coefficient.
This control strategy leads to a proportionality between the electromagnetic damping torque of the machine and the angular speed Ω_q. Hence, according to the control scheme, machine load impedances on the direct and quadrature axes can be evaluated as follow:

$$\begin{cases} R_{d,ext} = -\dfrac{V_d}{I_d} \\ R_{q,ext} = -\dfrac{V_q}{I_q} \end{cases}$$

where V and I are voltage and current values and, d and q subindexes indicate the direct or the quadrature axis. Because the direct current is ideally null, the direct axis is in open circuit. Thus only the quadrature axis, if $R_{q,ext}$, can provide energy regeneration, whose values can be calculated as

$$P_g = \frac{3}{2} R_{q,ext} I_q^2$$

.

Because of the difficulty in achieving all the variables needed and the power stage conduction and switching losses, obtaining P_g as described above can represent an issue: considering P_g as a power transfer from the motor phases to the DC bus the harvested power can be also computed as

$$P_g = V_{dc} Idc$$

2.3 Efficiency

The power conversion from the hydraulic domain of the pump to the electrical one required for battery supply is affected by different efficiency losses: volumetric, hydro-mechanical, electrical. The first term of loss if given by

$$\eta_v = \frac{V_g Q_g}{\Omega_g}$$

where Q_g is the pump flow rate, Ω_g its angular speed and V_g its fixed volumetric displacement.
The hydro-mechanical efficiency, due to rotating elements mechanical friction and hydraulic minor losses is

$$\eta_{hm} = \frac{T_m}{V_g \Delta P_g}$$

Where T_m is the electromagnetic torque of the motor and ΔP_g the pump pressure drop.
The third loss term is due to motor and power-stage losses in terms of conversion from the mechanical to the electrical domain because of the energy flow coming from the motor to the battery

$$\eta_e = \frac{V_{dc} I_{dc}}{T_m \Omega_g}$$

Where $V_d c$ and $I_d c$ are the voltage and current of the power stage DC bus.
Thus the total conversion efficiency of the motor-pump:

$$\eta = \eta_v \eta_{hm} \eta_e = \frac{V_{dc} I_{dc}}{\Delta P_g Q_g}$$

Experimental results show that a hydraulic shock absorber, implemented according to [2], is characterized the follwing behavior: the conversion efficiency, after reaching the maximum, drops, because of leakages and electrical losses. A quantitative analysis is presented in Tab. 2.1

Feature	Volumetric	Hydro-mechanical	Electrical	Total
avg	85.6	44	78.3	28
std	6	17.4	7.5	8.4
min	69.7	0	50.1	0
max	98.5	80	100	41.7
opt	85.5	62.4	78.2	41.7

Table 2.1: Statistic features of efficiency ([2]) average (avg), standard deviation (std), minimum (min), maximum (max) and optimal (opt). All the values are percentages.

In Fig.2.6 is noticeable how the maximum-efficiency region of the map can be achieved when if the control strategy prioritizes energy regeneration.

The maximum optimal value assumed by the conversion efficiency is of 41.7%. The hydraulic losses represents the 15% of the input power, electrical losses 12%, and hydro-mechanical losses, 32%, constitute the larger part of losses.

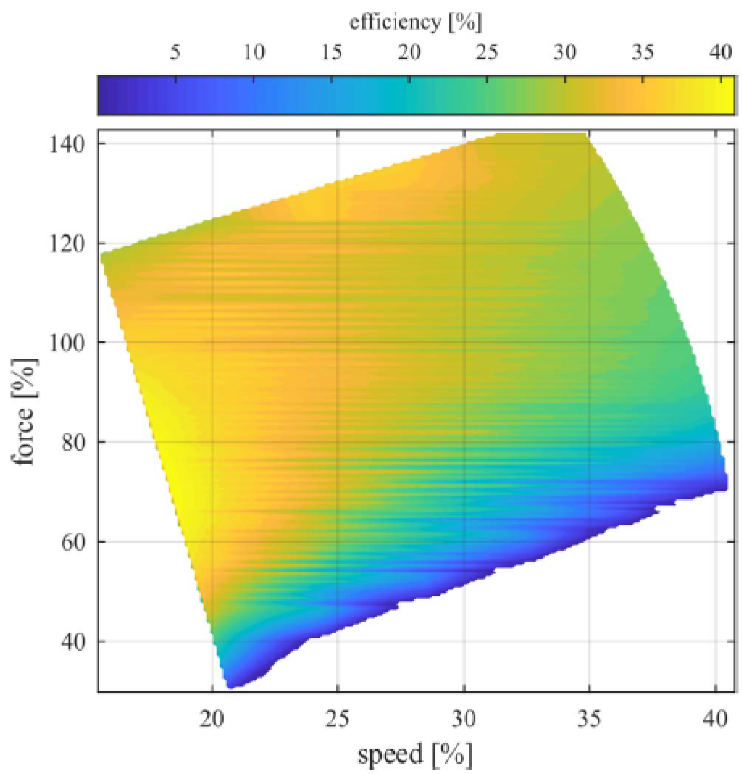

Figure 2.6: Experimental total conversion efficiency map of the motor-pump prototype. Axis units are normalized with respect to piston/damping force and speed ([2]).

CHAPTER 3

ENERGY MANAGEMENT

As already explained in the previous chapter, the mechatronic laboratory of the Polytechnic University of Turin developed a prototype of the regenerative shock absorber that exploits hydraulic, mechanical and electric subsystems.
It employs

- a conventional **twin-tube architecture**
- a **pump**
- **brushless machine** that, activated by the rotational movement produced by the pump, works as a current generator
- an **inverter**

Each of these elements represents an essential link in the power conversion chain (Fig. 3.1.a) contributing to the collection of the recovered power, but at the same time affects the final amount of recovered energy with its own efficiency.

The vibrational energy, produced by the shock absorber oscillation, flows, through the power chain, into the brushless machine and then by means of an inverter driven by a field oriented control becomes a DC current measurable on the inverter DC bus (Fig. 3.1. b-c).
The recovered power needs to be stored: a 48 V lead acid battery is thought as storage unit.

Hence hydraulic shock absorber design provides for a direct link between the inverter and the battery: it is necessary to analyze if the current used to feed the battery is suitable for charging purpose.

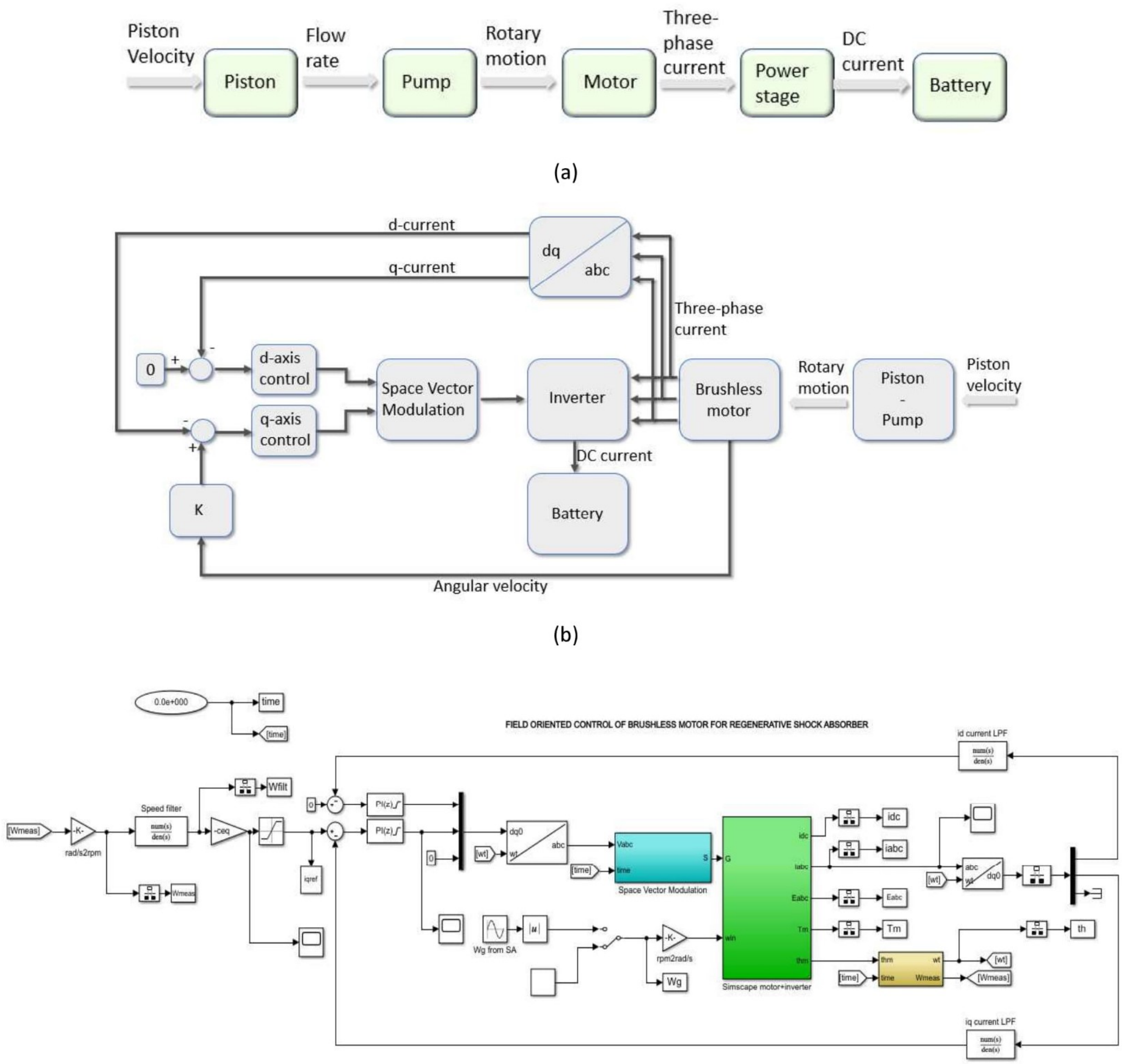

Figure 3.1: High view power conversion scheme of the regenerative shock absorber designed by the Mechatronic Laboratory of Polytechnic University of Turin (a). A more detailed block diagram focused on the flied oriented control for the brushless motor (b). The Simulink implementation of the regenerative active shock absorber

3.1 Recovered DC current analysis

In order to get a proper current evaluation is necessary to identify a suitable input angular velocity for the regenerative damper model. In his work, Mucka [14] presents an overview of the results, reached in the field of the energy harvesting potential of vehicle suspensions, and their limits. The bigger issue of this studies is the road condition: the road profile used are conforming to the road classes specified in ISO 8608 that are not well representative of current roads since their smoothness level derives from 1960/70s measurements.

Anyway, from the previous works listed in Mucka paper is possible to deduce a plausible relation between the road roughness coefficient, i.e. the road class, and the vehicle velocity: 120 km/h for class A, 50km/h for class C, and 30km/h for class D. These values are relevant not only for defining the environment needed to generate a proper motor angular velocity profile, but also for efficiency computation. In fact the suspension dissipates an average power proportional to the tire stiffness, the vehicle speed and the road roughness index defined by ISO as showed in Zuo and Zhang [15] work.
The following analysis has been done considering a condition that maximize the regenerative current: a C road profile (D profile is a very unlikely situation) with a vehicle speed of 50 km/h.
Sometimes also a motor angular velocity profile, generated on a C road profile and vehicle speed of 100 km/h, has been used with the only aim of verifying that the designed device has a good margin of working conditions.

The output current on the DC bus when the vehicle velocity on a C profile road is 50 km/h presents the shape showed in Fig.3.2

A more accurate analysis of the DC current reveals a peaks shape with the two major frequency components at 40kHz and 80kHz (Fig. 3.3).
This is due to the switching inverter frequency ($F_{sw} = 40kHz$), and to the space vector modulation used to drive the inverter (characterized by a sampling time $\Delta t = \dfrac{1}{2F_s}$ as explained in [16]).

An additional peculiarity of the DC bus current, that has revealed itself as irrelevant for the future design, was the presence of a small negative offset (about 1.6mA) caused by the losses of the power stage MOSFETs. Although in the present work the shock absorber movements generated on a C class road when the vehicle speed is 50 km/h has been mainly used, the two characteristic described above are common to different road profiles and to different velocities.

Because of his peaks shape the DC current can't be directly employed to charge a battery. It's neces-

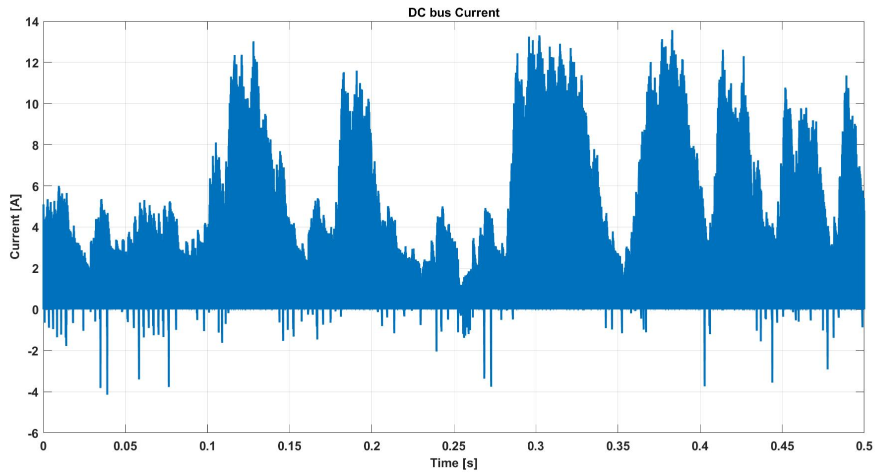

Figure 3.2: Evolution of the current on the constant voltage (48V) DC bus when the vehicle velocity on a C profile road is 50 km/h

sary the presence of a device able to smooth the current: the issue can be solved inserting a DC/DC converter in the conversion power chain (Fig.3.4).

As already mentioned, in [15], using the quarter car model, has been obtained a formula for the computation of the total amount of mechanical power dissipated by one shock absorbers:

$$P_{mech} = \pi^2 G_r v k_u$$

where G_r the road roughness index, v the vehicle speed [m/s] and k_u the tire stiffness. In case of a vehicle driving at 50 km/h on a C road profile

$$P_{mech} = \pi^2 25.6^{-7} \frac{50}{3.6} 226^3 = 79W$$

Applying a 40% efficiency due to the passage through the conversion power chain about 30W are expected do be at the chain output (Fig.3.5) for each shock absorber that lead to an overall output power of 120 W.

As first step for the converter design, some constraints has been defined as well as some simplifying hypothesis has been done:

- the voltage on the DC bus must be greater than 48V saving for voltage drops due to the presence of series resistances to the converter components;
- all the voltages must be upper bounded to 60V so that the device will not require extra tests but

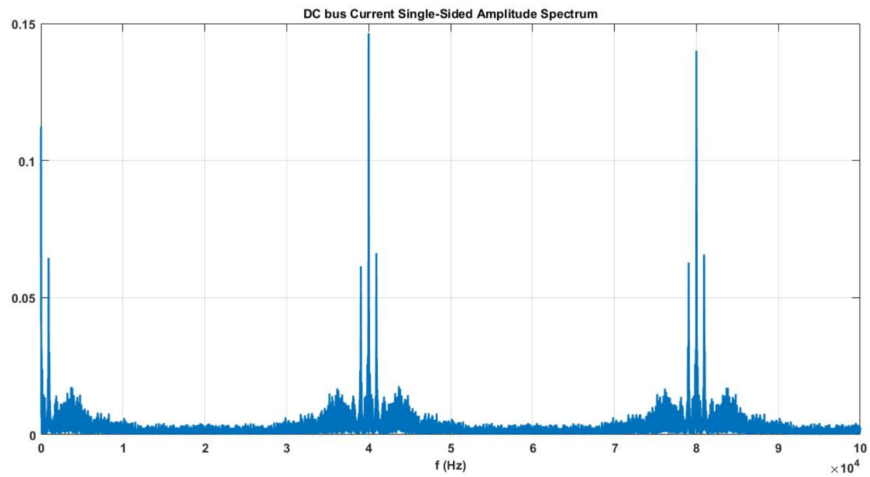

Figure 3.3: Frequency spectrum of the current on the constant voltage (48V) DC bus when the vehicle velocity on a C profile road is 50 km/h

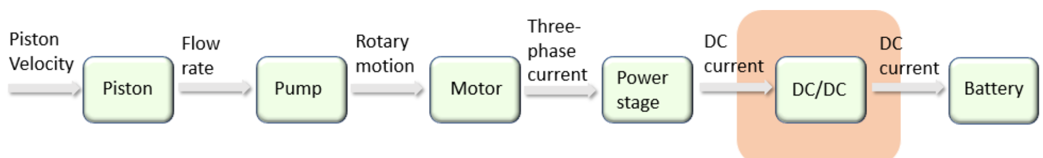

Figure 3.4: The DC/DC converter block has been added to the conversion power chain presented in Fig.3.1.a

could be part of the standard automotive ones;

- the current entering in the battery must be lower than one tenth of the battery capacity;
- the battery charging voltage should be greater than the battery voltage and lower than its float voltage;
- the battery has been considered as a constant voltage source, hence its SoC has been neglected for the converter design;
- the DC currents coming from each of the four active shock absorber must supply a single battery

To exploit the latter point it is necessary to define some possible configurations that can let the usage of a single battery. In particular two of them have been identified (Fig. 3.6).

In one case each corner is provided of a DC/DC converter and the four converters are connected in parallel to the battery. In the other case the four corners share a single DC bus that feed the only

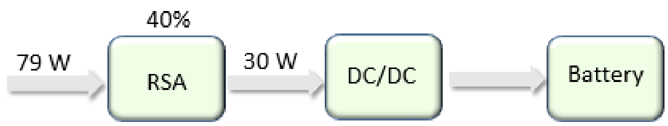

Figure 3.5: The regenerative active shock absorber designed in [2] is compacted in the RSA block presenting an efficiency of about 40%. In the figure the power flow generated by one shock absorber in case the vehicle is driving at 50 km/h on a C road profile is made explicit.

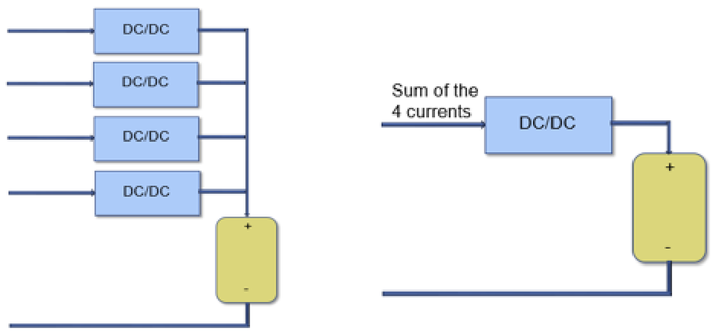

Figure 3.6: On the left the four DC/DC, one for each vehicle corner, connected to a single battery; on the right a single DC/DC, receiving the sum of the current coming from the motor of each shock absorber, connected to the battery.

converter and thus the battery. The choice between the two configurations can be taken by means of efficiency and cost analysis but for this purpose a more accurate design is needed.

An additional simplification used for the DC/DC design is given by the substitution of the entire hydraulic shock absorber model with a current generator, after all from the converter point of view the suspension system works as a current (positive or negative according to the brushless operational working mode) source.

3.2 Bidirectional voltage control

Since the presence of the converter cannot compromise the working functionality of the brushless machine, either as a motor, either as a break, a first approach has been that of considering the DC/DC as bidirectional device, and to split the design, so that to analyze one of its operational modes in isolation.
As showed in Fig.3.7, when the converter has to provide power to the motor-pump group, the DC/DC is a boost with a simpler feedback PID control.

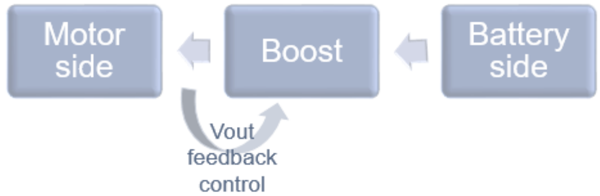

Figure 3.7: Conversion scheme overview when the brushless machine require current from the battery

The boost converter components values have been chosen as the common ones in the commercial DC/DCs:

- $C_{in} = C_{out} = 330\mu F$
- $L = 10\mu H$
- $R_{battery} = 1\Omega$
- $V_battery = 48V$

The standard topology has been modified inserting an extra switch, instead of the diode, so that the conversion device could actually be bidirectional (Fig. 3.8).

Moreover, the equivalent series resistances of the two capacitors and of the inductor has been ne-

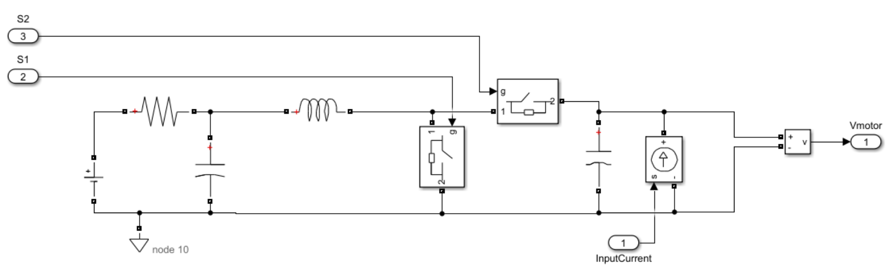

Figure 3.8: Bidirectional boost topology.

glected.

The PID controller has been tuned treating the device as a black box, in order to avoid the modeling, according to Ziegler-Nichols method. Choosing the V_{dc} on the bus a little bit higher than 48V the controlled system behaves as in Fig. 3.9.

When the power flows from the brushless machine to the battery, the converter, with the same topology described previously, can be seen as a buck converter with two possible control strategies (Fig.

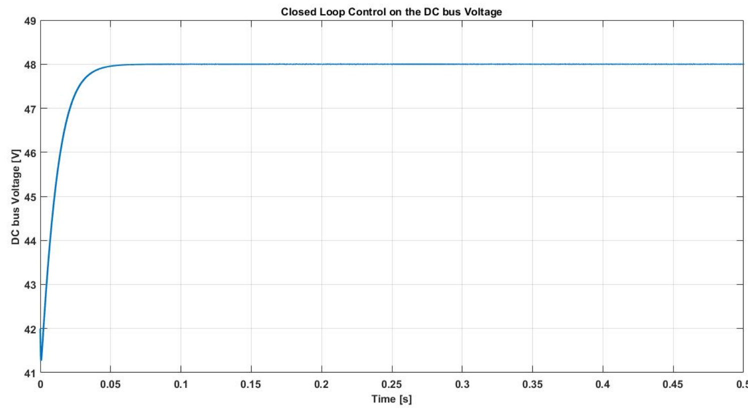

Figure 3.9: Feedback control response when the input current is -1A. The minus sign indicates that the current flows in the opposite direction of a charging current.

3.10), each to be combined with the one used when the electrical machine behaves like a motor: one is represented by a feedback control on the output voltage (on the battery side), the other by a feedforward control on the input voltage (on the motor side).

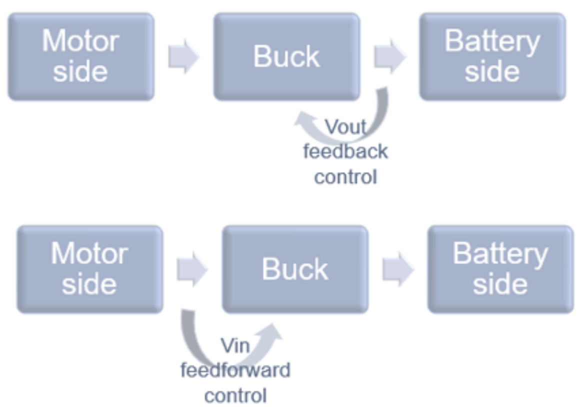

Figure 3.10: Conversion scheme overview when the brushless machine provide current to the battery.

In the former case the combination can be obtained with an extra control that identify the working mode of the brushless machine and thus selects which of the two controller the converter switches have to follow.

Although the feedforward control presents some limitation with respect to the feedback one, in this case offers the advantage of exploiting a single controller that drives only one switch, the one associate

with the converter type (buck or boost according to the working mode, identified by means of an extra control), while the other is left open.
In fact, the switch is actually a MOSFET that when is open behaves like a diode so that the DC/DC topology overlaps with the standard one. This more convenient options have been examined: the PID controller is the same used for the motor phase of the electrical machine, as well as converter topology, the only difference is of course represented by the swapping of the stitches driving signals (Fig.3.11).

The response to the input current obtained by the movement of a suspension belonging to a vehi-

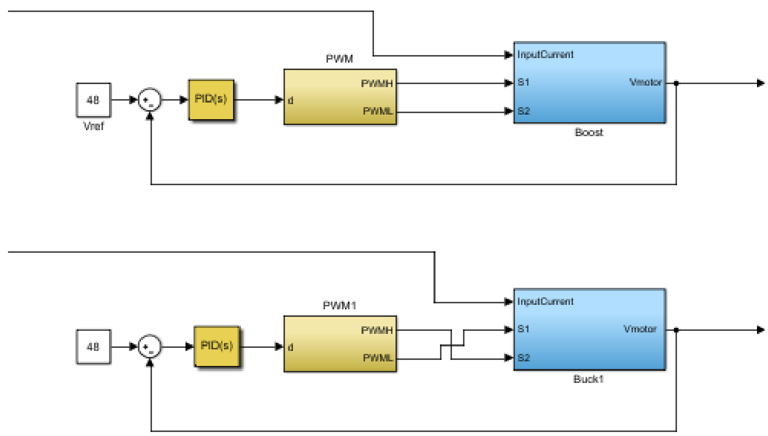

Figure 3.11: The two control schemes representing the same device in different working modes.

cle driving at 50 km/h on a C road profile is showed in fig. 3.12.

Since the controllers combining seems to be a complex solution and does not offers any guarantees about the current flowing into the battery, another approach has been preferred.

3.3 Feedback current control: Ziegler-Nichols design

There is the possibility of avoiding treating the converter as a bidirectional device exploiting an input capacitor enough big to provide energy to the brushless machine, when it's required, and to filter the input current giving a smoother shape.
Starting from an input value capacitor equal to $1mF$ a PID controller has been designed by means of Ziegler-Nichols method, but differently from the previous control scheme, the feedback signal is the output current, rather than the voltage. Assuming a constant reference is possible to identify two limit cases:

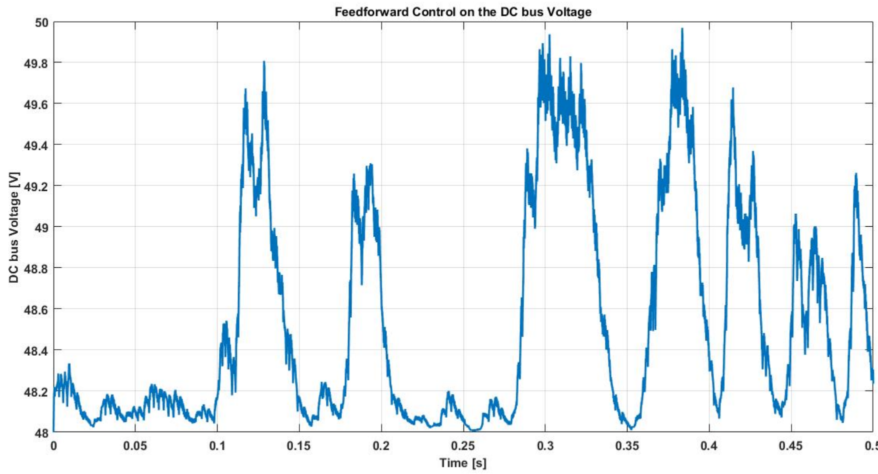

Figure 3.12: Feedforward control response on the voltage on the DC bus

- Very low reference current (order of 10^{-2}): it's implies a final constant current output but an increasing voltage profile that easily overcomes the limit of 60V.

- Very high reference current (order of 10^{1}): it's implies the impossibility to follow the reference for lack of input energy, hence there are no changes from the starting conditions, i.e. constant voltage on the bus, and a peaks shape currents.

It's clear that the reference signal cannot be a priori selected, since the converter output is greatly influenced by the input voltage values and must be a trade off between voltage and current smoothness. The first issue naturally leads to a proportional relation between the input voltage and the reference signal so that the trade off does not concern anymore the total reference but only the proportionality factor.
Before defining the proportionality factor value, it' important to note that the presence of the battery as output of the converter could alter the theoretical proportionality relation.
Assuming, for example, a null input current (no generation) we should expect a null input voltage, hence a null reference; this does not happen because the battery, the only power source, provides energy to the input capacitor whose voltage became the same of the battery one, saving for the voltage drop on the converter components. The battery can recharge the input capacitor by means of the recirculating current in the internal diode of the MOSFET. Current ricirculation is usually an unwanted phenomena but it let the DC bus to provide to the inverter-motor group always a voltage of at least 48V.

The control scheme has been designed as an internal current loop whose reference is the output of a proportional feed-forward control.

The proportional control input is the difference between the voltage on the input capacitor of the converter and the battery voltage, this means that it's only the part of the voltage on the input capacitor that is generated by the flowing of the regeneration current coming from the brushless machine (Fig.3.27).

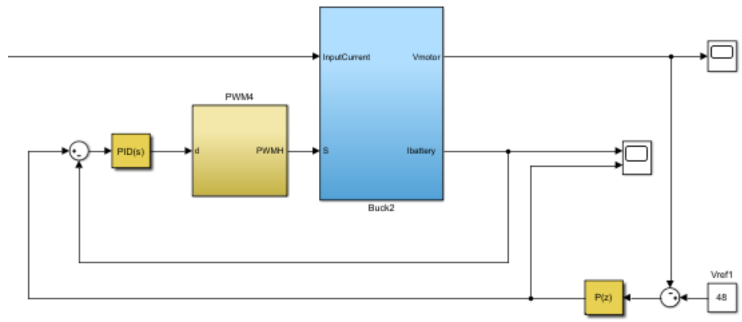

Figure 3.13: Overall control scheme: the feedback current control whose reference depends on the input voltage of the converter

Although the input capacitor value, set at the beginning of the section, provides good filtering property, the voltage at the input of the converter overcomes the limit of 60V for values of current comparable with the ones obtained as the sum of the currents coming from the four shock absorber (Fig.3.14). Hence the 1mF capacitor is effective only for low input current value, i.e. only for the case in which each shock absorber supply its own converter

Considering that none of the two configurations showed in Fig. 3.6 has still been identified as the best one, it's better to prevent to exclude the single DC/DC configuration. For this reason the input the 1mF capacitor has been replaced with a 10mF one that, besides, offers a better filtering.

Once the converter topology has been defined, it has been possible to find a proper proportionality factor.
It's has been set to the maximum value that guarantee the output current to be enough to follow the reference: this choice not only represent a trade off between a constant voltage (high frequency peaks shape current) and a constant current (high frequency peaks shape voltage), but also avoid the voltage on the capacitors to overcame the 60V limit.

The control scheme presented until now, is able to produce a smoother current shape of the battery but this is not enough to maintain safe the battery. A charge that does not damage the battery must provide a current smaller than one tenth of its capacity and a voltage smaller of its float voltage.
Monitoring both the output current and voltage could be resources consuming beyond that being a

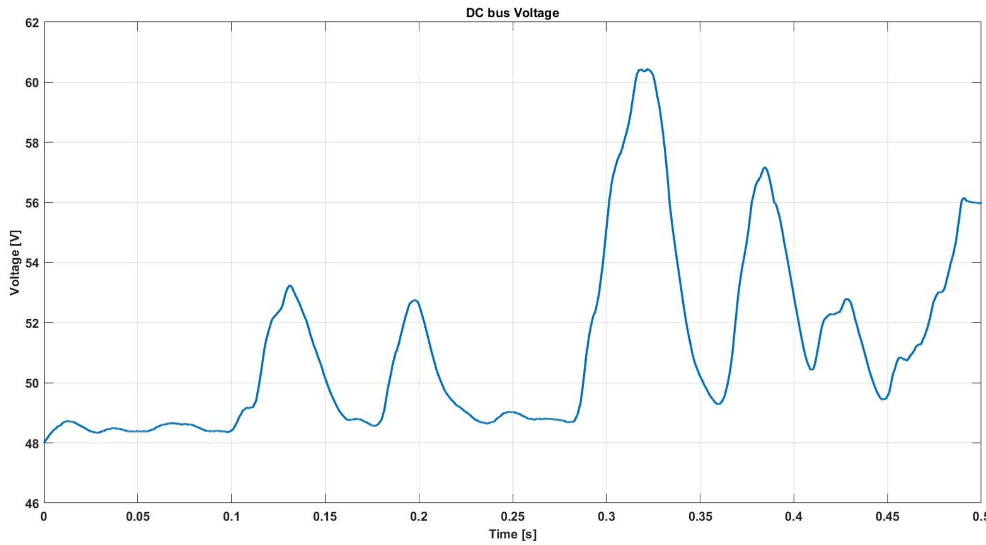

Figure 3.14: The evolution of the voltage on the DC bus

redundant operation. Actually, it is possible to compute the output voltage as function of the current (Fig.3.15):

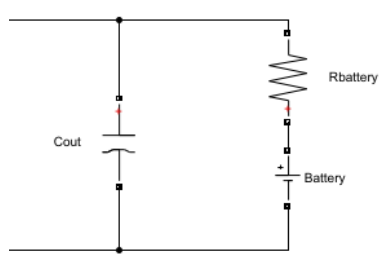

Figure 3.15: The circuit, representing the output of the converter, clearly shows how the capacitors and the battery with its series resistance are subjects to the same voltage, since they are connected in parallel. I_{out} is the current flowing in the battery and in the resistance.

$$V_{c_{out}} = R_{Battery} I_{out} + V_{Battery}$$

. If V_{float} is set as the maximum output voltage the corresponding output current is

$$I_{V_{float}} = \frac{V_{float} - V_{Battery}}{R_{battery}}$$

that implies $I_{out_{max}} = min(I_{Battery_{max}}, I_{V_{float}})$, where $I_{Battery_{max}}$ is the maximum current the battery can receive, i.e. one tenth of its capacity.

Using the most restrictive condition in term of current, it's possible to safeguard the battery modifying the control scheme and the converter topology: an extra control signal has been added to the output current (Fig. 3.16.

This signal drives a switch connected to a discharge resistance (Fig.3.17): when the voltage is so high

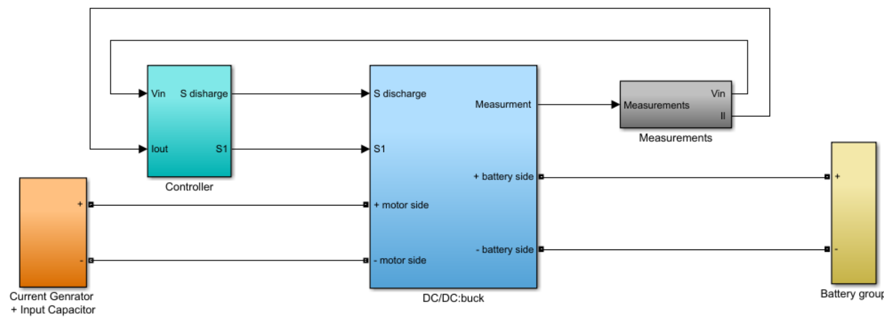

Figure 3.16: The circuit, representing the output of the converter, clearly shows how the capacitors and the battery with its series resistance are subjects to the same voltage, since they are connected in parallel. I_{out} is the current flowing in the battery and in the resistance.

to produce a current/voltage output that overcomes the limits previously imposed, the switch shuts, hence the input capacitor experiences a discharge that leads to a drop on the output signals.

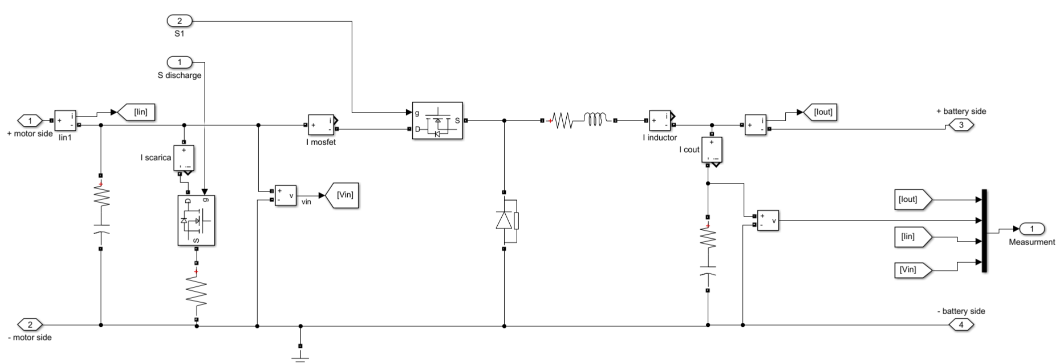

Figure 3.17: The buck topology has been modified adding an extra switch connected to a discharge resistance.

Assuming the condition imposed by the float voltage as the most restrictive one, the converter works as showed in Figg.3.18,3.19.

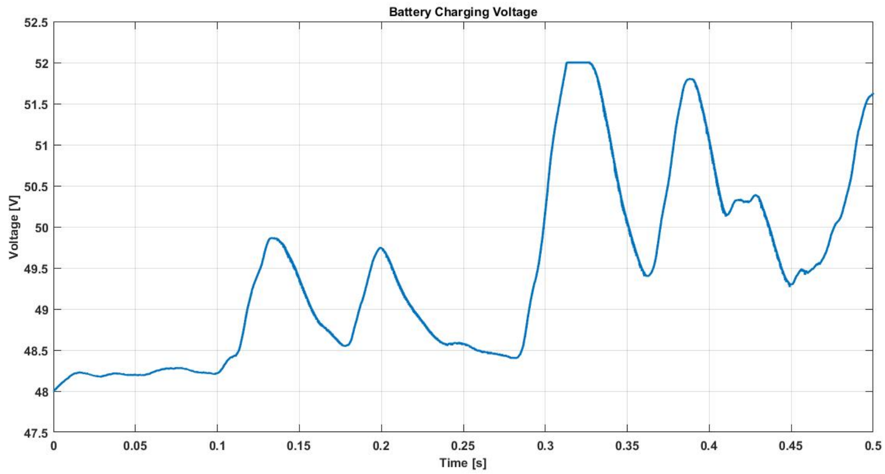

Figure 3.18: Voltage evolution measured on the output capacitor the converter.

3.4 Feedback current control: pole placement design

The capacitors and the inductor used in the converter until now are ideal components, but it has been necessary to realize a more realistic model of the device: series resistors have been added to each components.

Although the PI controller has been designed treating the converter as a black box, the DC/DC has anyway a transfer function that link the duty cycle to the output current for which that PI controller is clearly suitable. The ESRs presence implies the modification of this transfer function, and thus, the worthlessness of the controller (Fig.3.20).

In order to make the control action effective it has been necessary to design a more structured controller starting for the modelling of the buck converter.
A quite simple modelling method is the State Space-Averaging one. As explained in ([17]), the State-Space Averaging method is demonstrated to be an effective technique to describe the small-signal line whose aim is to characterize the transfer properties of a DC/DC converter.
Before proceeding, some modifications to the original buck topology have been done only for modelling and controller design purposes (it means that no changes will be applied to the real configuration designed until now). From the converter point of view (Fig3.21), the current generator and the capacitor actually represent a random voltage generator whose output value is $v_g(t)$, and the battery load can be seen as a simple resistance whose value has been defining exploiting the result obtained in the

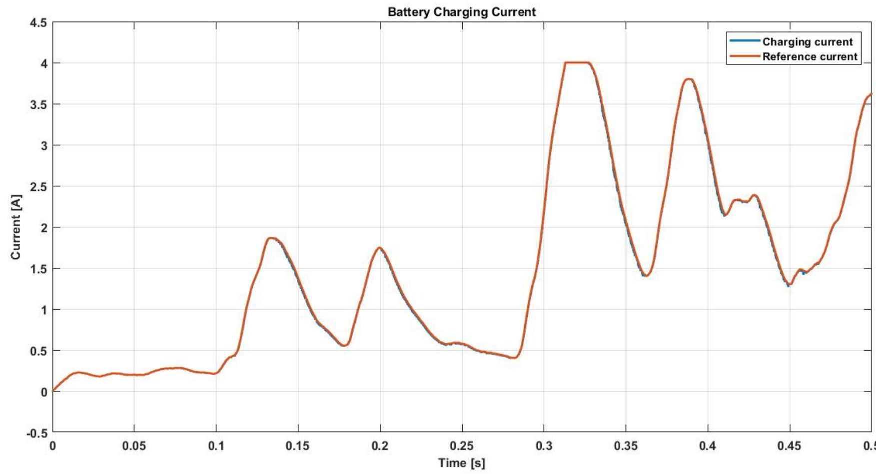

Figure 3.19: Current evolution in input to the battery.

previous paragraph:

$$R = \frac{V_{foat}}{I_{v_{float}}}$$

It's actually possible to divide the switching period of the converter, T_{sw}, in a T_{ON} time, during which the converter is in conduction mode, and a T_{OFF}, during which behaves like an open circuit (Fig. 3.22).
Hence only two state variables,the inductor current i_L and the output capacitor voltage $v_{C_{out}}$, define the system behavior in each time interval.

A LTI system can be represented as follows:

$$\dot{x} = Ax + Bu$$

where

$$x = \begin{bmatrix} i_L \\ v_{Cout} \end{bmatrix}$$

Assuming to be d the duty cycle, during $T_{on} = T_{sw}d$ the converter behavior can be described by

$$\dot{x} = A_{ON}x + B_{ON}v_g$$

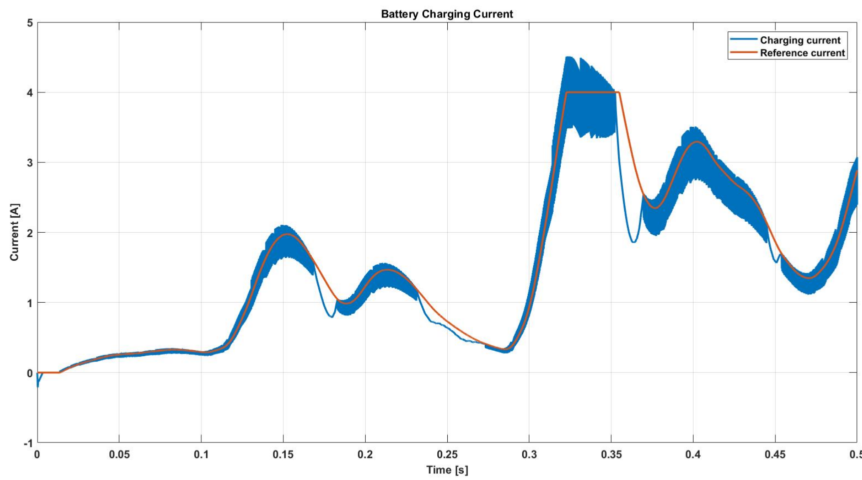

Figure 3.20: Beyond the current ripple, the output current does not follow properly the reference.

where

$$A_{ON} = \begin{bmatrix} \frac{-(ESR_L + ESR_{C_{in}} + R||ESR_{C_{out}})}{L} & \frac{-R}{L(R+ESR_{C_{out}})} \\ \frac{R}{C(R+ESR_{C_{out}})} & \frac{-1}{C(R+ESR_{C_{out}})} \end{bmatrix} \qquad B_{ON} = \begin{bmatrix} \frac{1}{L} \\ 0 \end{bmatrix}$$

during $T_{on} = T_{sw}d$ the converter behavior can be by

$$\dot{x} = A_{OFF}x + B_{OFF}v_g$$

where

$$A_{OFF} = \begin{bmatrix} \frac{-(ESR_L + R||ESR_{C_{out}})}{L} & \frac{-R}{L(R+ESR_{C_{out}})} \\ \frac{R}{C(R+ESR_{C_{out}})} & \frac{-1}{C(R+ESR_{C_{out}})} \end{bmatrix} \qquad B_{OFF} = \begin{bmatrix} 0 \\ 0 \end{bmatrix}$$

The average combination of these two equations systems leads to a single state-space description of the converter razing the switching ripple of the state variable:

$$\dot{x} = Ax + Bv_g$$

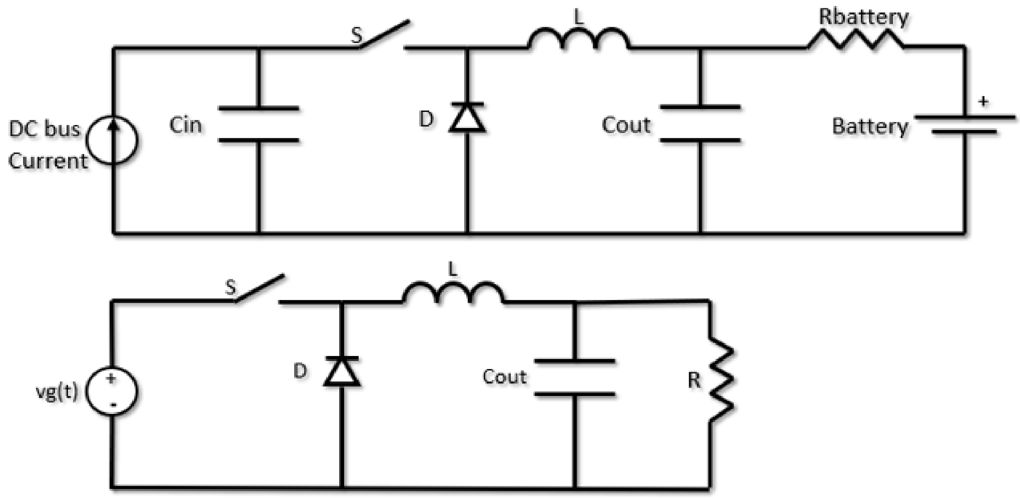

Figure 3.21: The top schematics represents the actual buck topology, the other one shows its modifications for the modelling purposes.

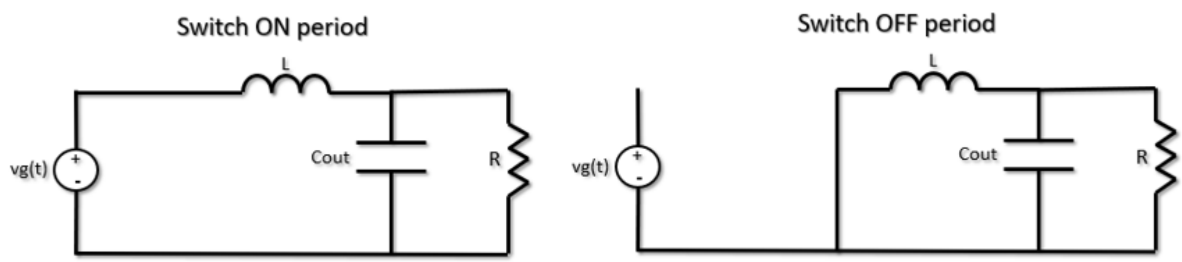

Figure 3.22: The schematics show the buck circuit respectively during T_{on} and T_{off}. The voltage generator not connecting to anything during the OFF period does not create issues since it's only a representation: it actually is a current generator in parallel with a capacitor.

where

$$A = A_{ON}d + A_{OFF}(1-d) = \begin{bmatrix} \frac{-(ESR_L + dESR_{C_{in}} + R||ESR_{C_{out}})}{L} & \frac{-R}{L(R+ESR_{C_{out}})} \\ \frac{R}{C(R+ESR_{C_{out}})} & \frac{-1}{C(R+ESR_{C_{out}})} \end{bmatrix}$$

$$B = B_{ON}d + B_{OFF}(1-d) = \begin{bmatrix} \frac{d}{L} \\ 0 \end{bmatrix}$$

Since the matrices A and B may be dependent by the duty ratio, i.e the averaged equation may be non-linear with respect to duty, in order to achieve the final aim of providing an equivalent linear circuit, the signals have been analyzed considering little perturbation around the operating point:

$$d = D + \hat{d}$$

$$x = X + \hat{x}$$

$$y = Y + \hat{y}$$

$$v_g = V_g + \hat{v}_g$$

The capitalized letters represent the steady state values of the signals while the carets represent the small perturbations. The steady state operating point has been founded setting the time derivative to zero as well as the perturbation terms $\hat{x}$ and $\hat{v}_g$:

$$AX + bV_g = 0$$

whose solution is

$$X = -A^{-1}BV_g$$

By means of the steady state values the linearized general equation of the ac small signal model, obtained discarding the non-linear (second-order) terms, is

$$\dot{\hat{x}} = A\hat{x} + B\hat{v}_g + [(A_{ON} - A_{OFF})X + (B_{ON} - B_{OFF})V_g]\hat{d}$$

The expression displayed the two inputs of the system: the line voltage generator $\hat{v}_g$ and the duty ratio $\hat{d}$. The system response to the variations in the duty cycle modulation term is given, exploiting the linearity properties, setting $\hat{v}_g = 0$:

$$\dot{\hat{x}} = A\hat{x} + [(A_{ON} - A_{OFF})X + (B_{ON} - B_{OFF})V_g]\hat{d}$$

The equations have been solved in the frequency domain by means of the Laplace transform:

$$s\hat{i}_L = -\left(\frac{ESR_L + ESR_{C_{in}}D + R||ESR_{C_{out}}}{L}\right)\hat{i}_L - \frac{-R}{L(R + ESR_{C_{out}}))}\hat{v}_{C_{out}} + \left(\frac{V_g - ESR_{C_{in}}I_L}{L}\right)\hat{d} \tag{3.1}$$

$$s\hat{v}_{C_{out}} = \frac{R}{C_{out}(R + ESR_{C_{out}})}\hat{i}_L - \frac{1}{C_{out}(R + ESR_{C_{out}})}\hat{v}_{C_{out}} \tag{3.2}$$

The resulting transfer function $\frac{\hat{i}_{out}}{\hat{d}}$ from the duty ratio to inductor current is obtained from (3.1) and

(3.2) is:

$$G_{id}(s) = \frac{\hat{i}_{out}(s)}{\hat{d}(s)} = \frac{V_g - ESR_{C_{in}}\hat{i}_l}{sL + ESR_L + ESR_{C_{out}}D + (R||ESR_{C_{out}}) + \dfrac{R^2}{sC_{out}(ESR_{C_{out}}+R)^2 + (ESR_{C_{out}}+R)}} \tag{3.3}$$

It's evident how the transfer function depends on the ESRs values, thus before proceeding is necessary to define capacitors: in compliance with ripple values imposed by the components the desired input capacitance has been obtained by the parallel of three $3.3mF$ capacitors, the output capacitance by the parallel of three $150\mu F$ capacitors, and the inductance using a $22\mu H$.
The controller design requires to multiply the (3.3) for the transfer function of the PWM modulator, that is characterized by no phase delays, no zeros, no pole, i.e simply for a gain equal to $\frac{1}{V_{triangle}}$, where $V_{triangle}$ is the highness of the modulation signal used for the PWM. The Bode diagram is showed in Fig.3.23. The desired open loop gain, $|G(s)|$, is a straight line with a slope of $-20dB/dec$

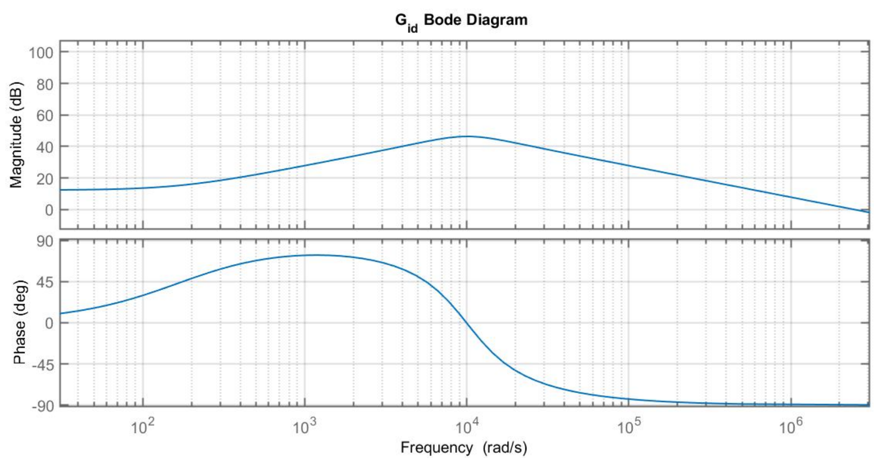

Figure 3.23: Bode diagram of the(3.3).

and a frequency crossover f_c, at least equal to $\frac{1}{2}f_{sw}$ in order to respect Nyquist theorem, where f_{sw} is the switching frequency of the converter. Actually the f_c has been chosen as a trade off between system speed and noise rejection, equal about to $\frac{1}{4}f_{sw}$.
The straight line can be identified by the general equation $y = mx + q$, where $m = -20$ and, substituting to x and y the coordinates of a known point $(0, \log_{10} f_c)$, $q = 20\log_{10} f_c$. The static gain of G(s), K_{dB}, is also equal, by definition, to q. Applying the final value theorem

$$\lim_{s\to 0} sG(s) = \lim_{s\to 0} sGc(s)Gp(s) = \lim_{s\to 0} sK_p\frac{Kc}{s} = K_pK_c = K$$

$$\Rightarrow K_c = \frac{K}{K_p}$$

where $G_c(s)$ represents the controller transfer function and K_c its static gain.
Writing $G_c(s) = \frac{K_c}{s} G_c'(s)$, $G_c'(s)$ can be founded looking to the Fig.3.24 in which the magnitude diagram of $G_c(s)$ has been simply drawn: pole placement has been performed considering that $G_c'(s)$ must have a unitary gain.

The final open loop gain, obtained by means of the controller $G_c(s)$, can be observed in Fig.3.25, and

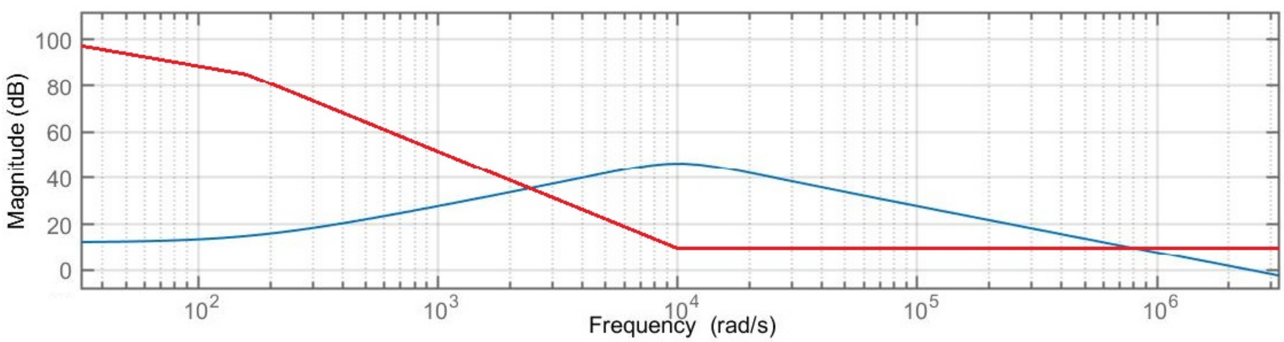

Figure 3.24: The magnitude diagram of $G_c(s)$ has been simply drawn in red on the bode diagram of $G_{id}(s)$.

the total system response to different reference signals is promising(Fig. 3.26).

The validity of the controller must be verified only in a global simulation that takes into account the real converter topology, and not only his mathematical model, considering the overall control scheme (Fig. 3.27).

3.5 Regenerative shock absorbers: concurrent work

Once the final topology of the converter and its controller has been defined, a comparison between the two configurations (Fig. 3.6), that take into account the four corner charging a single battery, can be done.
The evaluation has been performed according the following terms:

- efficiency
- cost
- actual feasibility

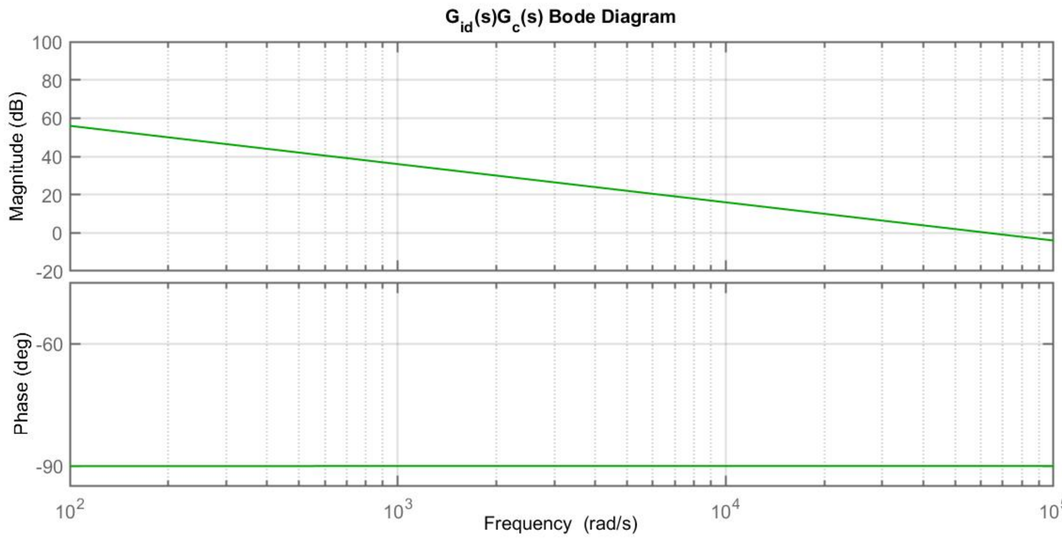

Figure 3.25: Bode diagram of the open loop gain.

The efficiency term clearly depends on the amount of current flowing on the components series resistor but is also affected by the switch closing of the discharge resistance: the most the resistance is connected to the rest of the DC/DC the most is the efficiency loss. Therefore, the presence of the discharging resistance plays a fundamental role in favor of the configuration with a single DC/DC.
In fact when the single converter is considered, as previously explained, $I_{out_{max}}$ is equal to the $min(I_{Battery_{max}}, I_{V_{float}})$; instead in the 4 DC/DC case the current value that drive the switching closing is $min(\frac{I_{Battery_{max}}}{4}, I_{V_{float}})$: this means that there is an higher probability to be $I_{out_{max}} = \frac{I_{Battery_{max}}}{4}$, hence in cases of great unequal distribution on the four DC/DC one of the discharge switch could be closed because is providing a current bigger than $\frac{I_{Battery_{max}}}{4}$, generating an efficiency loss, although the total voltage current on the battery is less than $I_{Battery_{max}}$.

Considering the currents coming from the four shock absorber identical instant by instant, and the devices power input computed as the product of the current on the DC bus and the voltage on the input capacitor, the efficiency obtained as the ratio between average output power and average input power of the converter is 67% for the 4-DC/DC configuration, and 82% for the 1-DC/DC configuration.

These efficiency results can be roughly explained splitting the power losses of the converter in two categories: proportional to the current squared, and constant. Thus for the 4-DC/DC configuration $P_{L_4} = 4R_{eq}\left(\frac{I_{DCbus}}{4}\right)^2 + 4c$, while for the 1-DC/DC configuration$P_{L_1} = R_{eq}I_{DCbus}^2 + c$, where R_{eq} is

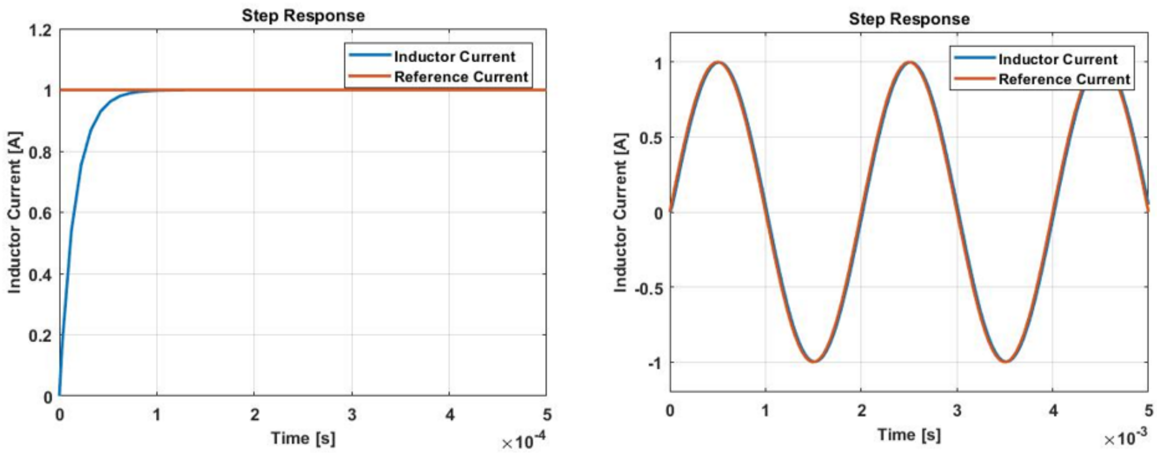

Figure 3.26: Response to the unitary step with initial time $t_0 = 0s$ on the left, and to a 100Hz sine wave on the right.

not a real resistance but an equivalent term used to represent all the losses depending by the current squared and the c term represents the constant losses with respect to the current flowing into the converter (Fig. 3.28).
Considering that the average current value is small and that the constant therms c are the same, P_{L_1} is lower than P_{L_4}

Also, the cost analysis supports the single DC/DC: the presence of four DC/DC quadruplicates the costs without offering any kind of redundancy since the controller is based on a current loop and the four converters have been connected in parallel.

Moreover the 4 DC/DC configuration could present some feasibility difficulties, in fact the 4 converters could easily affect each other during the working operation creating undesirable situations.

In conclusion the most convenient configuration is the one in which a single converter, fed by the pump-motor group of each shock absorber, charges the battery; hence all the simulation results showed as follow are obtained considering the four corners exploiting one DC/DC (Fig.3.29).

3.6 Results and operational limitations

In order to make the simulations more realistic, voltage drops on the lines that connect the inverter of each shock absorber to the converter input port, have been added.

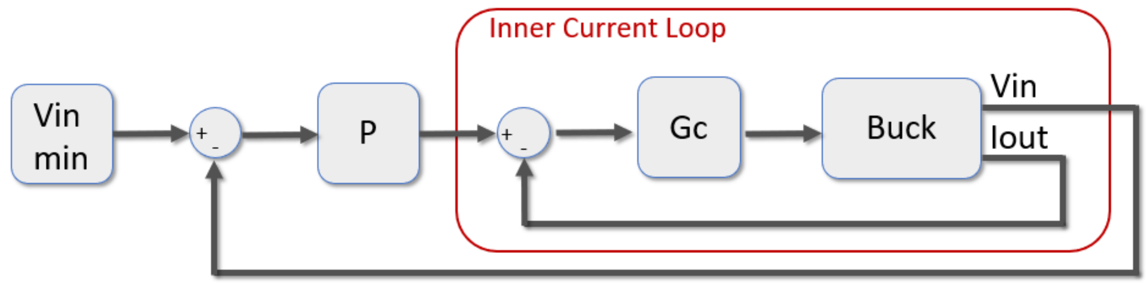

Figure 3.27: Block diagram of the converter control, where $V_{in_{min}}$ is the desired minimum value on DC bus that allows the flow of current into the battery, i.e. the switch closure; P is the proportionality factor used for the computation of the reference for the current control; G_c is current controller developed performing the pole placement; the Buck block represents the plant whose transfer function is G_{id}

.

In particular the final simulation model consists in four lines, each with a 2Ω resistance whose terminals are connected to one side to the parallel of a current generator and a capacitor of 1mF, and the other to the input capacitor of the converter (Fig.3.30).

When the converter is fed with the current coming from the four suspensions of a vehicle driving at 50 km/h, on a C road profile, the input battery and voltage presents acceptable trends with respect to the starting ones (Fig.3.31)
Considering the obtained results, it's necessary to understand if current and voltage, provided by the buck converter, are suitable for the battery charging.
There is no a constraint about imposing constant charging voltage and/or current, in fact among the different method to charge a lead acid battery, some of them contemplate constant current, some constant voltage, some non constant either current, either voltage. There are anyway ripple limits that need to be verified.

In the constant float voltage charging method there are strict restriction about the voltage ripple; is no the ripple per se causing problem but the overcoming of the float voltage value ([10]). In this study case the charging voltage is not constant but never overcomes the 52V limit because of the controller (actually there is a good margin since the maximum admissible output current corresponding to the 52V is 4A and the 4A limit is imposed to the inductor current).

The ripple can be more easily observed and measured in the case in which the angular velocity of the brushless machine is constant as in Fig. 3.32: the saw-tooth ripple on the output current reach a maximum rms value is 0.1 A.

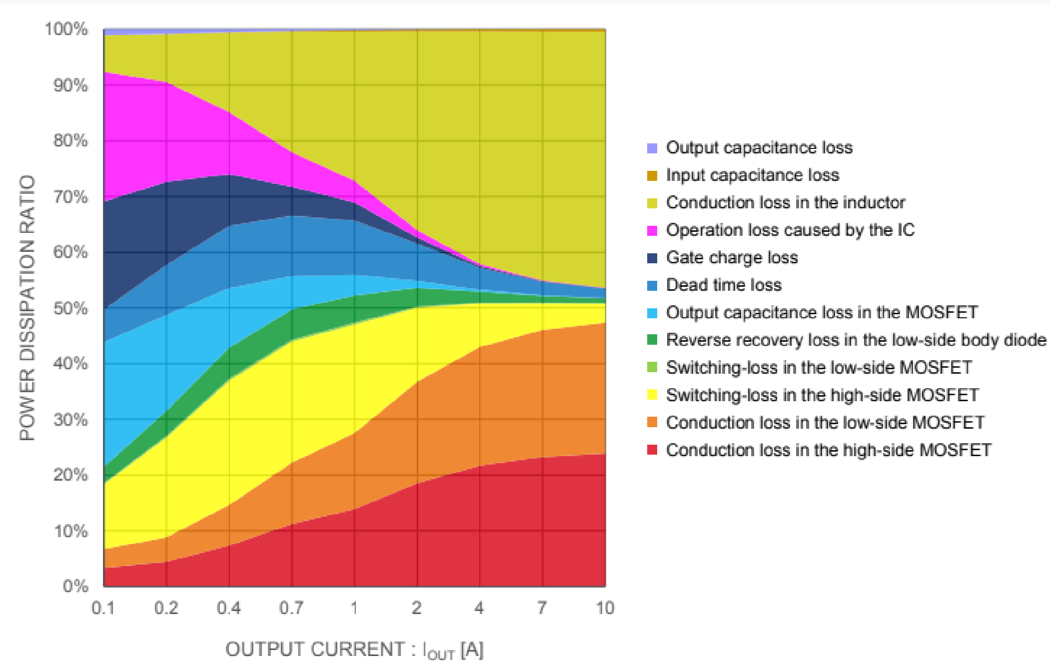

Figure 3.28: Percentage partitioning of the power dissipation with respect to the output current. The evaluation showed in figure concerns a two side buck converter ([18]).

From the figure it is also noticeable that the ripple amplitude increases with the increasing of the output current value, thus, considering that according to the controller impositions, the maximum current value flows to the battery when the inductor current is 4 A, hence when the discharge switch is closed (Fig. 3.31, current graph, about in the time range between 3 and 3.5 s), it's possible to affirm that the battery input current presents at most a 0.15 A rms ripple.
If for 100Ah battery capacity the maximum rms ripple value is 5A ([10]), the obtained current evolution is acceptable (Fig 3.33).

Once the energy management device functioning has been proved, the current generators, used to recreating the effect of the regeneration by means of the shock absorbers, have been removed, and the DC/DC with his controller has been directly connected to the simulation model used in [2] (Fig. 3.34)

The presence of the converter does not affect the suspension control system working, in fact the input current to the DC/DC does not show great differences with respect to the simulation in which the motor-pump group is directly connected to the battery (Fig. 3.35).
This means that although the converter is almost transparent from the motor point of view, is able to provide suitable charging condition to the battery. The converter does not creates issues for the

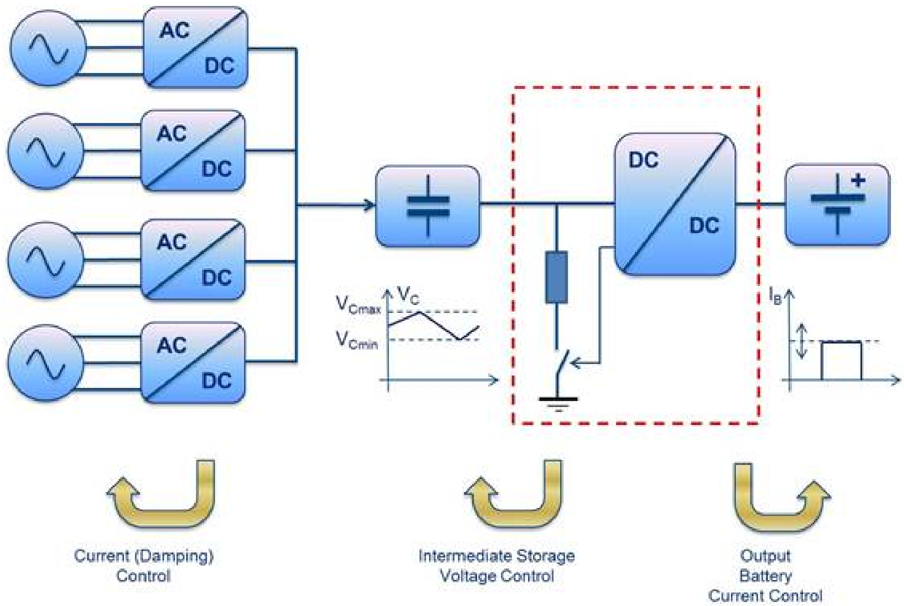

Figure 3.29: High vision model.

inverter motor group since the DC bus is always provided for at leas 48 V.

Actually it's possible to set an higher value for the bus voltage: until the predefined value is not reached the buck switch remain open letting the input capacitor to charge. The voltage level could be easily increased changing one controller variable.
The current reference will be computed as proportional to the difference between the current voltage value on the bus and the minimum voltage level that allows the current to flows into the battery. In other words the reference coverter output current is zero until the desired value of voltage on the DC bus is not raised.
Raising the minimum voltage value for starting the battery charge means providing energy to the battery only when the floating voltage, for example, is achieved. Anyway this could lead to an easier crossing of the 60V limit or to the waste of recovered energy in fact, if the floating voltage value is never raised during a single drive, all the power collected will be consumed because of the input capacitor self-discharge. A proper evaluation should be done according to SoC of the battery, the vehicle velocity and the road profile, thus, along this work, the minimum voltage value of the bus that allows the switch closure has been decided to remain 48V.

A final simulation to prove the functionality of the converter has been performed using two models of the brushless machine control (Fig. 3.36) in order to verify the overall functionality of the

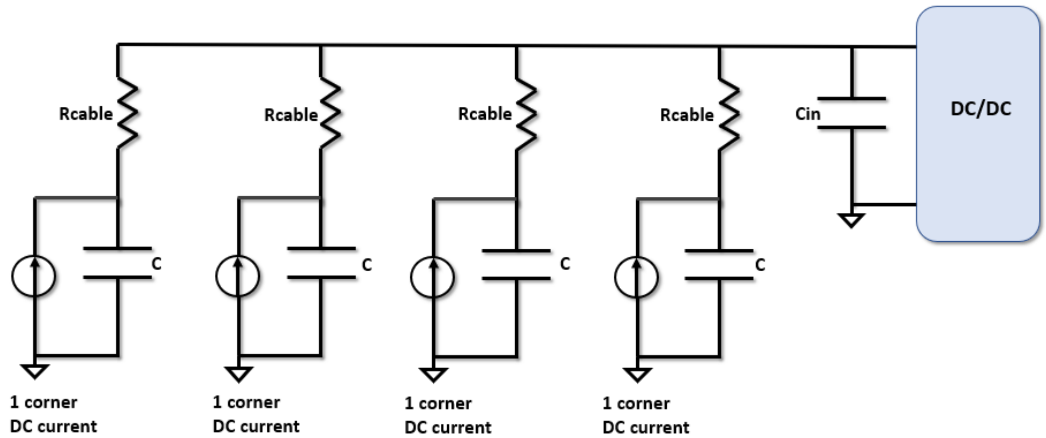

Figure 3.30: More realistic simulation model.

converter when is fed with the currents coming from two shock absorbers, one front, one rear (Fig. 3.37).

There are some limit situations to be taken into account: when the car is stopped, and the active functionality of the suspension is employed lifting the chassis, the devise is not able to provide enough energy.
The average power required for 10 seconds lifting is 40 W, thus a huge capacitance is required. An approximate calculation can be done, assuming the constant voltage bus (48V):

$$4P = V_{bus} I_{bus} \Rightarrow I_{bus} = \frac{4 * 40W}{48V} = 3.33A$$

Reminding the charging low of a capacitor

$$C = \frac{1}{V_{bus}} \int_t I_{bus} dt \Rightarrow C \approx 700mF$$

Since the obtained value is not feasible, an extra link between the DC bus and the battery should be needed.
In simulation this connection is provided by the internal MOSFET diode that let the current flowing from the battery to the DC bus. During real prototype development it's better to exploit an additional diode meant to be for the battery-DC bus connection; in this way, anytime the input capacitor cannot provide the energy required by the motor on the bus (e.g. for lifting functionality), the brushless machine can work as motor thanks to the energy directly supplied by the battery.

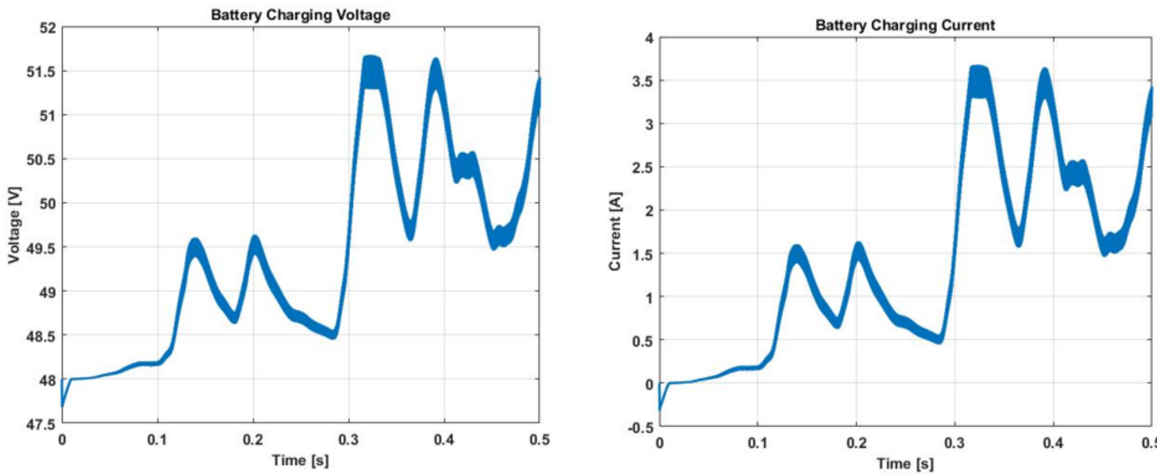

Figure 3.31: Converter output voltage and current evolution.

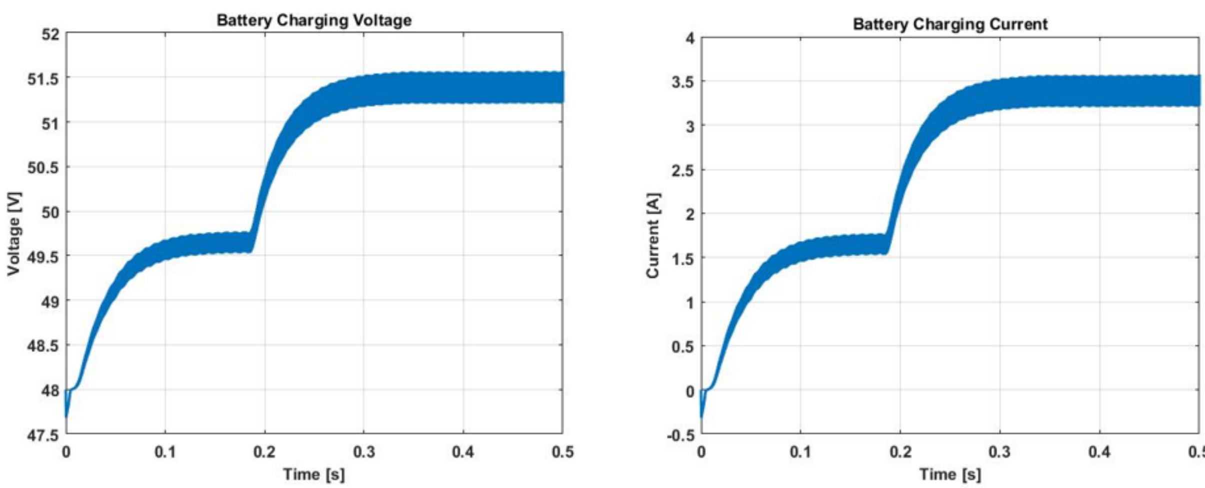

Figure 3.32: Converter output voltage and current evolution when the angular velocity of the brushless machine is constant and equal to 140 rad/s.

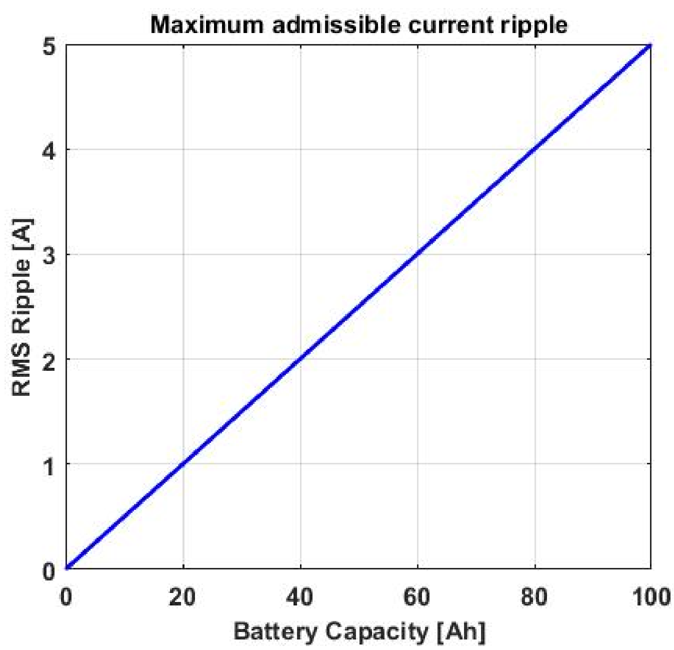

Figure 3.33: Ideal relation between battery capacity and maximum admissible current ripple.

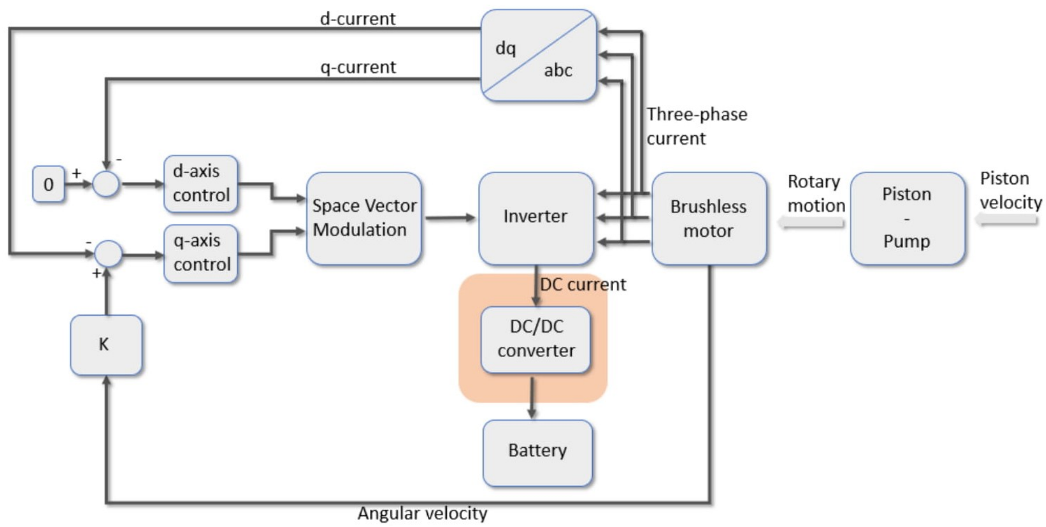

(a)

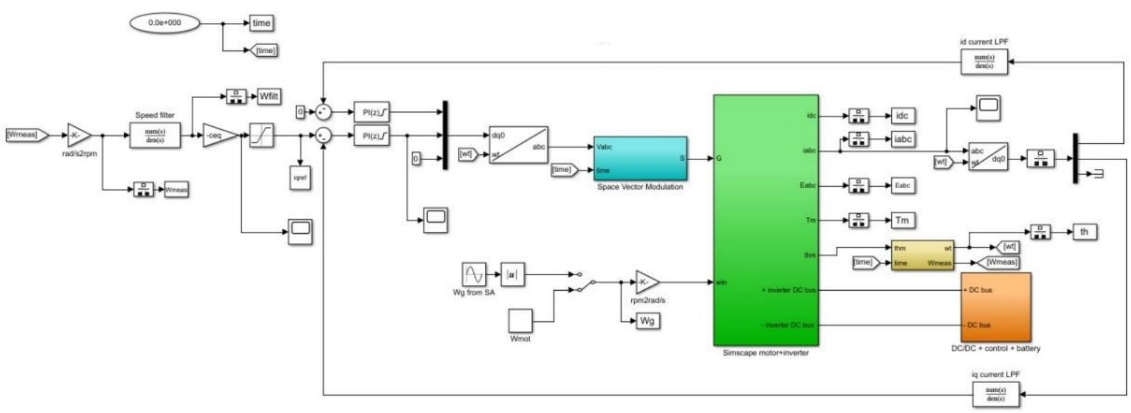

(b)

Figure 3.34: The designed DC/DC converter is connected to the field orieneted brushless motor control for regenerative shock absorber developed in [2]: field oriented control block diagram (a), Simulink scheme (b). The figure should be compared with Fig. 3.1

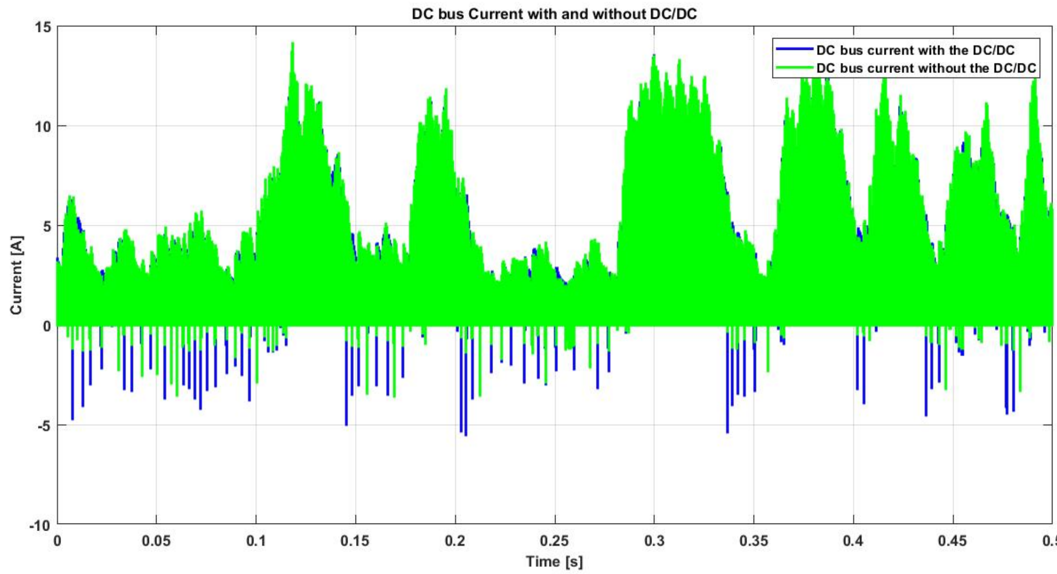

Figure 3.35: Comparison between DC bus current: the green line shows the evolution of the current on the DC bus when 1 shock absorber is directly connected to the battery; the blue one shows the evolution of the current on the DC bus when two shock absorbers, one front and one rear, are connected to the battery by means of the DC/DC converter .

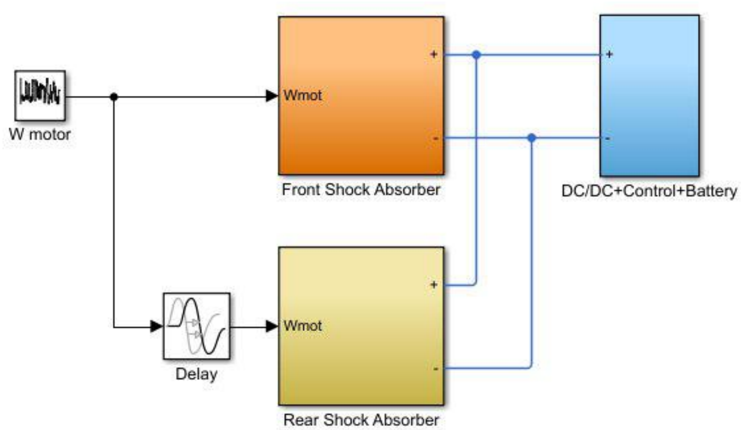

Figure 3.36: Simulink scheme of the overall model: only two shock absorbers, one front and one rear, according to the single track model, are connected to the battery by means of the DC/DC. The motor angular velocity signal coming from the rear suspension has been obtained delaying the angular velocity signal of the front shock absorber. The delay value has been computed as the ratio between the longitudinal length of the Jeep Renegade (2.57 m) and the vehicle speed (100 km/h ≈14 m/s)

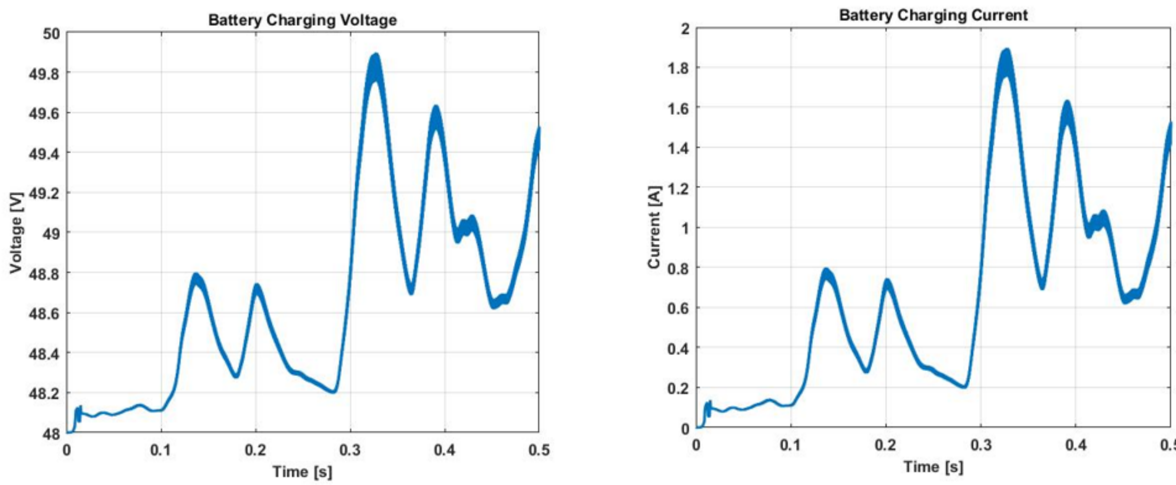

Figure 3.37: Converter output voltage and current evolution when two shock absorbers, one front and one rear, are connected to the battery by means of the DC/DC.

CHAPTER 4

DESIGN VALIDATION

4.1 Model simplification

The converter and its controller design has been evaluated and validated in Simulink simulation environment. In order to get an ulterior worth confirmation of the controller working principle a test has been performed on a real simpler device (with respect to the one designed), made up of a resistive load, connected to the output inverter capacitor by means of a switch.
Ideally the buck converter behaves like a DC transformer:

$$V_{dc_bus} = aV_{dc_{load}}$$

where V_{dc_bus} is the voltace on the inverter DC bus, a is the transformation factor that is practically obtained as a resistance whose value is weighted by the switch, and $V_{dc_{load}}$ is the average voltage measured on the load resistor.

The structural differences between a DC/DC coupled with a battery and its high view version are causes of control loops changes.
Although, the control strategy is unvaried except from the controller type: a PI standard controller for the inner current loop is enough valiant. (Fig. 4.1).

The PI parameters of the inner loop have been tuned by means of the open loop Ziegler-Nichols method. The external feed-forward control receives as input only the input voltage: in this simpler configuration the battery presence has been neglected, thus the subtraction of the two voltages characterizing the controller of the complete converter has no meaning.
Also in this case the proportionality factor has been chosen as a compromise between a too high value, that leads to the controller failure because of lack of enough input current, and a too low value that

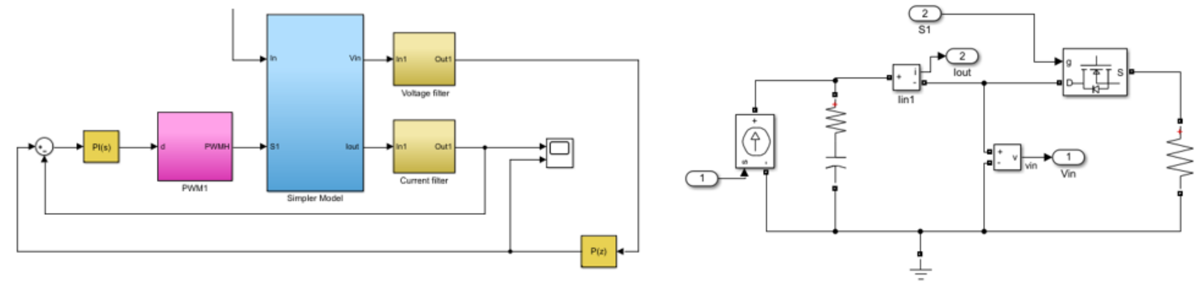

Figure 4.1: Simpler Simulink model.

could cause the capacitor overload.

The presence of two filter on the measured quantities used for the control represent a news with respect to the complete DC/DC controller design. The two filters, especially the output current one, are essential for control purpose, in fact the resistor, on which the regeneration current is discharged according to the switch closure, behaves only on average like a DC/DC converter: the output current is a square wave modulated on the shape of the input voltage, but the control loop considers only the filtered current flowing on the resistance, that is actually proportional to the input voltage.

The simulation results of this scheme are showed in Fig.4.2.

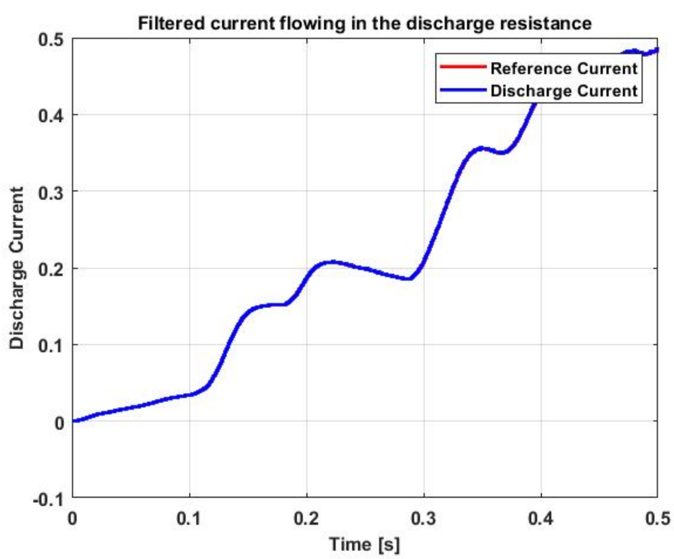

Figure 4.2: Simplified model controller response when the input current is the one generated on a C class road profile at 50 km/h.

4.2 Multipurpose power module

The multipurpose power module or MPPM has a key role in the regenerative shock absorbers power stage.
An integrated power module processes power according to the information content at the control interface. Functions that are covered by integrated power modules include power supply bus types, passive components integrated into the bus and passive components integrated into the load, among others. An integrated power module provides the physical containment package for several power components, usually Power semiconductor devices.
It is equipped with a DSP TMS320F28335 produced by Texas Instrument. The DSP is characterized by a C28x CPU, a maximum operating frequency of 150 MHz, 512 kB flesh memory and 68 kB RAM. It provide for 16 ADC channels with 12 bit resolution, 12 PWM channels, 6DMA channels, 88 GPIO and works in a temperature range of -40 to 125 C.

The MPPM used in [2] consist in two three-phases inverters (six switches and the corresponding diodes for each inverter) connected through a common bus (Fig. 4.3).

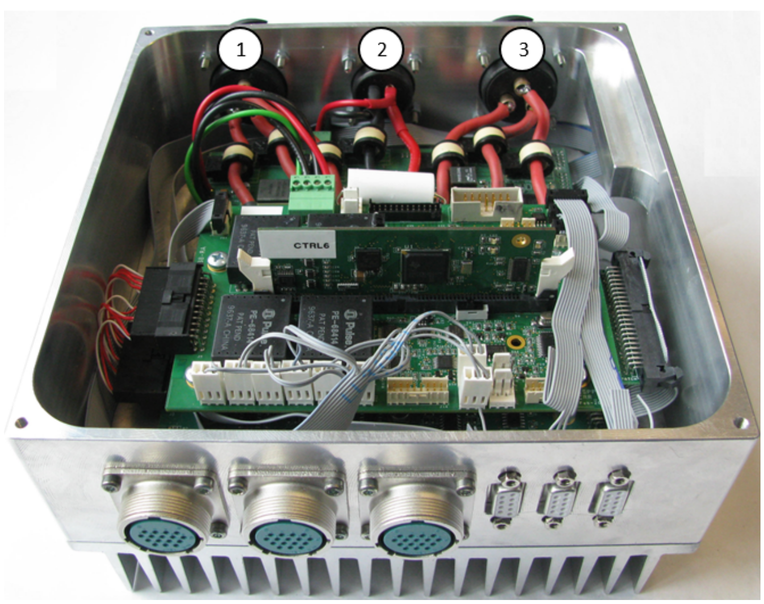

Figure 4.3: The three phases of each inverter, u v w, are distinguishable in figure (1),(2), as well as the DC bus in the middle (3).

The MPPM is associated with a vehicle axle shaft, thus the two iverters are meant to be connected to the brushless motors of the two shock absorbers, on left and one right.
For the purpose of this chapter only one shock absorber controller has been tested, therefore one of the phases, in particular its high side switch, of the unused inverter has been exploited as the switch that connect and disconnect the load resistance according to the controller.

4.3 Controller code

The integrated environment used for the development, and compiling of the controller code is Code Composer Studio, an Eclipse based environment, compatible with the DSP of the multipurpose power module.
The code used for the space vector modulation, i.e. for the inverter control in the regenerative shock absorber in [2], has been slightly modified for the in order to have a new control function that implements the PI control.
The code recycling, beyond several advantages, has created also some issues.
The main one is current and voltage sampling. In a first attempt the new control and filters were characterized by a sampling frequency equal to the motor inverter switching one. According to the preexisting current control the ADC interrupt was activate simultaneously with the PWM signal collecting only one output current sample, on the falling edge, in each period, leading to a falsification of the current measure and consequently to the worthless of the control.
A solution is represented by the reduction of the controller sampling frequency (Fig.4.4), but also the duty updating must have the same occurrence frequency in order to avoid useless or even dangerous intermediate duty updating (Appendix B).

4.4 Validation

The software let also the observation and the evolution of the variables used in the code and modify some of them at run time.

The controller evaluation has been performed step by step. The multi purpose power module has been connected at first to a power source only for supply purpose so that to verify the correctness of the filter implementation.
Then the controller functionality have been evaluate connecting one phase of one inverter to the load resistance and the DC bus to a constant voltage in order to simulate a constant regeneration voltage although the other inverter connected to the shock absorber is let in idle state.

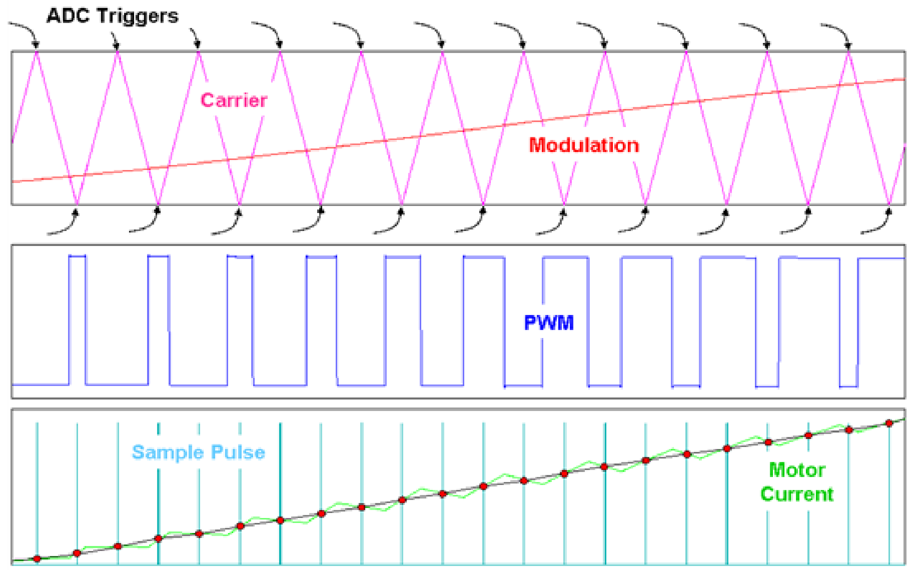

Figure 4.4: The ADC trigger higher frequency let to collect more the one sample for each PWM period.

Finally six 1mF capacitors have been soldered in parallel and connected, still in parallel, to the DC bus and the entire regeneration system has been tested. By means of a drill, the brushless motor has been made run and the three-phase produced current has been transformed into DC current by means of one of the two inverter, activating the field-oriented control developed in [2] (Fig.4.6). The DC current, flowing on the DC bus, is filtered by the capacitance and discharged on the load resistance according to a switch (implemented by the high side of the other inverter) closure (Fig 4.5).

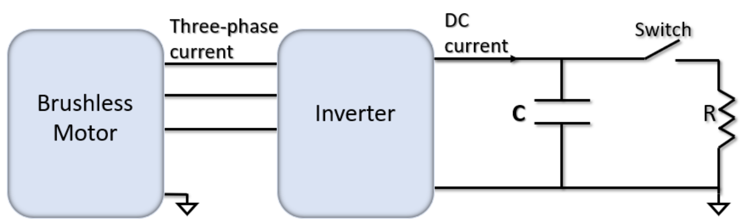

Figure 4.5: Circuital schematic of the test set up.

The employment of non ideal devices highlights the importance of the DC bus voltage filter: the low cutting frequency avoids dangerous noise loops due to the recursive usage of the DC voltage (in proportional term) as input current reference.

The controller response is showed in Fig.4.7.

An actual comparison with the simulation model has not been possible because of the difficulty in

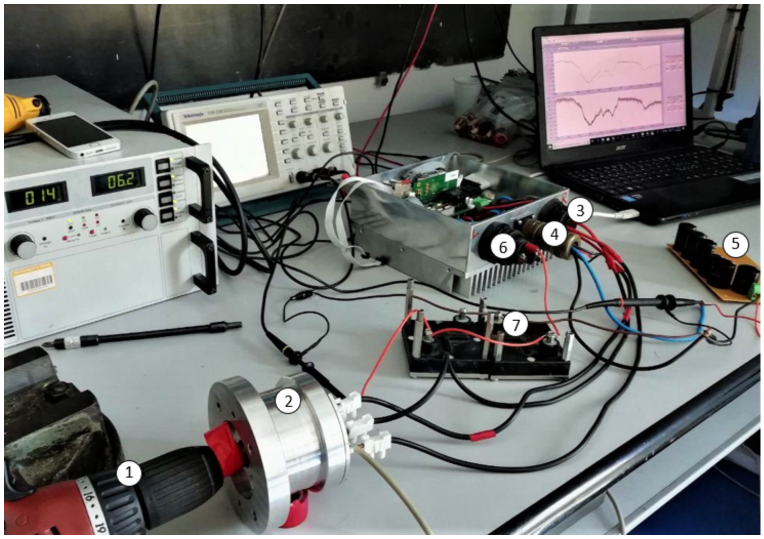

Figure 4.6: Test set up. Drill (1), brushless motor (2), three-phase inverter (3), DC bus (4), capacitors (5), discharge switch (6), discharge load resistance (7).

simulating the motor movement produced by the shock absorbers working by means of a drill.
Anyway the test displays the correct functionality of the control strategy and thus validates the high view version of the converter designed in the previous chapter. In fact, not only the filtered current discharged on the load resistance follows the reference imposed by the voltage on the DC bus, but also the brushless motor does not suffer the presence of the converter, or at least its equivalent resistance, since the voltage on the DC bus increases with the increasing of the angular velocity as it would do without the converter. Moreover similarities with the simulation can be observed: constant angular motor velocity leads to constant DC bus voltage both in simulation and reality.

Fig. 4.7 shows a low voltage level of the DC bus. This can be explained by the absence of the battery: the voltage value on the input capacitor of the converter is provided by the only power coming from the brushless motor.
Recalling the control scheme presented in Fig. 4.1, it's evident how the discharge on the load resistance starts as soon as the DC bus presents a voltage level greater than zero. A minimum value of the DC bus voltage, before which the switch remain open letting the charging of the capacitor, can be set as showed in Fig. 4.8. .
The results obtained with the new control scheme (Fig. 4.9), more similar to the original one designed for the buck converter, presents an effective raised level of voltage on the DC bus and a lower current flowing on the discharge resistance. The decreasing current is due to a decreasing value of the difference between the minimum DC voltage set by the controller and the actual voltage on the bus. .

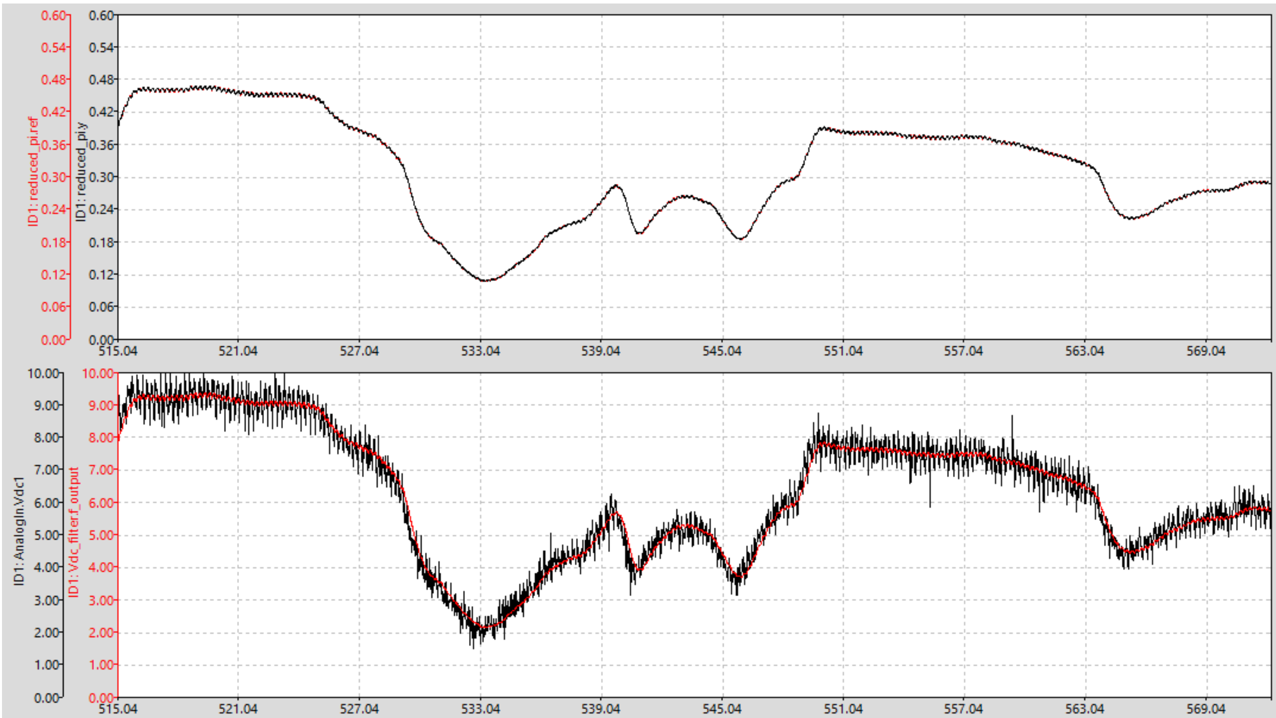

Figure 4.7: Test result visualization. The upper graph shows the controller working comparing the reference signal with the system output. In the lower graph is displayed the filtering operation on the DC bus voltage.

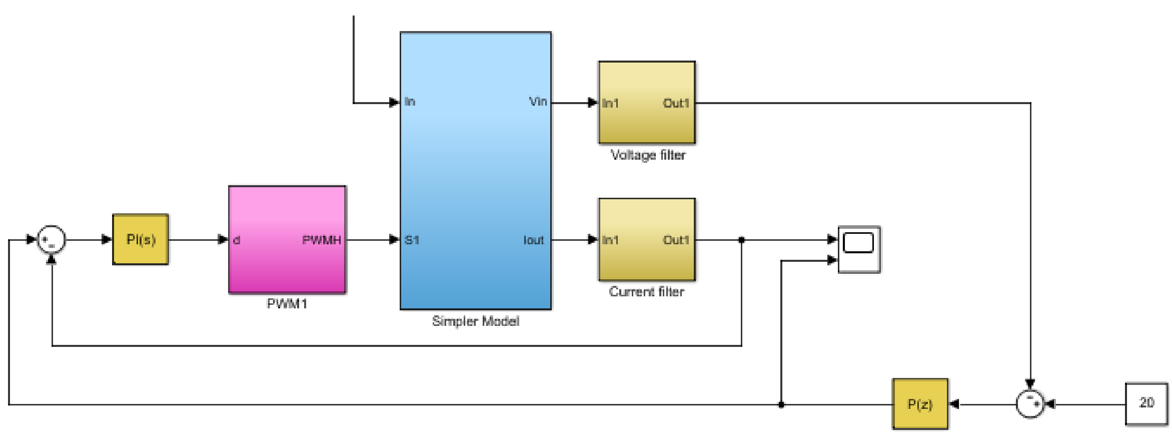

Figure 4.8: The minimum value of the DC bus voltage is added to the previous control scheme.

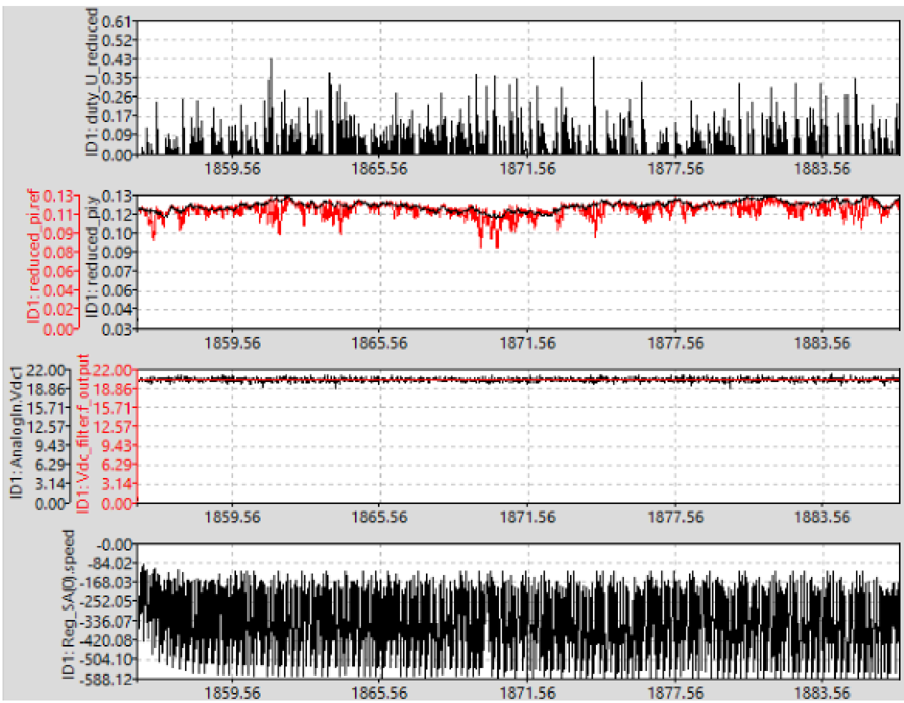

Figure 4.9: The minimum value of the DC bus voltage is added to the previous control scheme.

CHAPTER 5

CONCLUSION

5.1 Summary

The present thesis work describes in detail the process for the design of a device that, fed with energy provided by regenerative shock absorbers can supply a 48V lead acid battery. The device has been identified to a be a DC/DC buck converter whose controller has been developed following an inductive approach.

Once the converter components have been properly selected and the controller defined, it has been possible to identify the best configuration that could let the four shock absorber to charge a single battery.
The analysis has been performed in term of efficiency, costs and feasibility and it reveals how the coupling of the battery with a single converter fed with the energy coming from the four suspensions is most suitable solution.

Results presented at the end of chapter three show the worthiness of the device and how it is compliant with the imposed constraints. Moreover a simplified version of the final device has been realized in order to perform an high view test for the validation of the control strategy and the examination of the brushless motor reaction to the presence of the DC/DC converter.
The test has been conducted connecting the brushless motor to a discharge load resistance by means of a multipurpose power module.

5.2 Efficiency Results

The regenerative shock absorber prototype developed by the mechatronic laboratory of Polytechnic University of Turin is charcterized maximum conversion efficiency of 41.7% [2].
Considering a road profile that maximize the regenerative current (C class road profile) and a vehicle velocity of 50 km/h the efficiency of the battery charging device is 82%, thus the overall regenerative shock absorber efficiency is 34.2%. The hydro-mechanical losses have been identified as the most critical aspect of the total design.

5.3 Future applications

Although Simulink simulations and high view test show positive results before to mount the designed device on commercial cars other tests, on the complete design, must be accomplished.
There are, also, enhancements that could be done in the design: as already mentioned charging performances could be improved by the usage of a SoC additive loop that could increase or decreases V_{float}. It should be noted that what is called V_{float} is not properly the floating battery voltage, since it is a varying value, but the maximum voltage allowed for the battery charging for a fixed SoC.

Furthermore it's evident how the recovered power cannot be the only power source for the battery charging because of its random time evolution. The SoC control gives the possibility of computing the instantaneous battery power need and providing for the part of power that could not be eventually supplied by the regenerative mechanism from an extra power source. Thus the SoC control loop could prevent also the battery to be undercharged.

The integration the regeneration devices on commercial cars in mass production is a long way, but at present the powertrain electrification represents the most immediate solution to the limitation of vehicle noxious emission.

BIBLIOGRAPHY

[1] Uwe Kiencke, Lars Nielsen *Automotive Control Systems: For Engine, Driveline, and Vehicle*,Chapters 3 and 5. Springer Science & Business Media, 5 dic 2005

[2] Renato Galluzzi, Yijun Xu, Nicola Amati, Andrea Tonoli *Optimized design and characterization of motor-pump unit for energy regenerative shock absorbers*. Elsevier Ltd., 29 October 2017.

[3] Galluzzi R, Tonoli A, Amati N, Curcuruto G, et al. *Regenerative shock absorbers and the role of the motion rectifier*. SAE paper 2016-01-1552; 2016.

[4] Yaser M. Roshan, Amir Maravandi, and Mehrdad Moallem *Power Electronics Control of an Energy Regenerative Mechatronic Damper*.IEEE TRANSACTIONS ON INDUSTRIAL ELECTRONICS, VOL. 62, NO. 5, MAY 2015.

[5] Zhen Longxin, Wei Xiaogang *Structure and Performance Analysis of Regenerative Electromagnetic Shock Absorber*. JOURNAL OF NETWORKS, VOL. 5, NO. 12, DECEMBER 2010

[6] Zhongjie Li et al *Energy-harvesting shock absorber with a mechanical motion rectifier*. 2013 Smart Mater. Struct. 22 025008.

[7] Zutao Zhang, Xingtian Zhang, Weiwu Chen, Yagubov Rasim, Waleed Salman, Hongye Pan, Yanping Yuan a, Chunbai Wangc *A high-efficiency energy regenerative shock absorber using supercapacitors for renewable energy applications in range extended electric vehicle*. Elsevier, Applied Energy 178 (2016) 177–188

[8] Kawamoto Y, Suda Y, Inoue H, Kondo T. *Electro-mechanical suspension system considering energy consumption and vehicle manoeuvre*. Vehicle System Dynamics, Vol. 46, Supplement, 2008, 1053–1063.

[9] Andrea Tonoli , Nicola Amati , Joaquim Girardello Detoni , Renato Galluzzi, Enrico Gasparin (2013). *Modelling and validation of electromechanical shock absorbers*, Vehicle System Dynamics, 51:8, 1186-1199, DOI: 10.1080/00423114.2013.789538.

[10] J. Allen Byrne, *THE PROPER CHARGING OF STATIONARY LEAD-ACID BATTERIES. (YOUR BATTERY IS ONLY AS GOOD AS HOW YOU CHARGE IT.)* Engineering, Training and Tech Support Manager Interstate PowerCare, a Division of Interstate Batteries. Dallas, TX

[11] Guntur Harus Laksana and Syuhri Skriptyan N. H. *Analysis d the battery state of charge and electric generator influence on the dynamic characteristic of hydro-magneto-electric regenerative shock absorbers*. ARPN Journal of Engineering and Applied Sciences, VOL. 13, NO. 1, JANUARY 2018.

[12] Bing Xie, Yiqi Liu, Yanchao Ji, JianzeWang *Two-Stage Battery Energy Storage System (BESS) in AC Microgrids with Balanced State-of Charge and Guaranteed Small-Signal Stability*. Energies 2018, 11, 322; doi:10.3390/en11020322

[13] Asep Nugroho, Estiko Rijanto, Latif Rozaqi *Buck Converter Control for Lead Acid Battery Charger using Peak Current Mode* International Journal of Power Electronics and Drive System (IJPEDS) Vol. 8, No. 2, June 2017, pp. 686 694 ISSN: 2088-8694, DOI: 10.11591/ijpeds.v8i2.pp686-694

[14] Peter Múčka *Energy-harvesting potential of automobile suspension, Vehicle System Dynamics*. DOI: 10.1080/00423114.2016.1227077

[15] Zuo L, Zhang PS. *Energy harvesting, ride comfort, and road handling of regenerative vehicle suspensions*. J Vib Acoust 2013;135(1):011002.

[16] Joseph P John, Dr. S. Suresh Kumar, Jaya B. *Space Vector Modulation based Field Oriented Control Scheme for Brushless DC Motors*.PROCEEDINGS OF ICETECT 2011.

[17] W.M. Polivka, P.R.K. Chetty, AND R.D. Middlebrook, *State-Space Average Modelling of Converters with Parasistic and Storage-Time Modulation*. 1980 IEEE.

[18] ROHM semiconductor, *Efficiency of Buck Converter*, December 2016 - Rev.001, AEK59-D1-0364-0.

Appendices

APPENDIX A

MATLAB SCRIPT

In this appendix there is the MATLAB script used for the computation of the current loop controller G_c.

```
clear all
close all
clc
s=tf('s');

L=22e-6;
C1=9.9e-3;
C2=450e-6;
%Esr1=0;
Esr1=1/(1/(50e-3)+1/(50e-3)+1/(50e-3));
Esr2=1/(1/(300e-3)+1/(300e-3)+1/(300e-3));
Esr3=140e-3;

Vout=52;
Vin=54;
Iout=4;
R=Vout/Iout;
D=Vout/Vin;

A=[-(Esr3+D*Esr1+R*Esr2/(R+Esr2))/L -R/(L*(R+Esr2)); R/(C2*(R+Esr2)) -1/(C2*(R+
    Esr2))];
B=[D/L; 0];
x=-pinv(A)*B*Vin;
```

```
il=x(1);

a=R/(s*R*C2+s*Esr2*C2+1);
Gi_d=zpk(minreal((Vin/L-Esr1*il/L)/(s-Esr2*a/((Esr2+R)*L)+a/L+Esr3/L+Esr2*R/(L*(R+
    Esr2))+Esr1*D/L),0.01));
figure, bode (Gi_d),grid on, title ('G_{id} Bode Diagram')

Kc=62832/dcgain(Gi_d);
Gc=Kc*(1/Gi_d)/(dcgain(1/Gi_d)*s);

figure, bode (Gi_d),grid on, hold on, bode(Gi_d*Gc,'r')
```

APPENDIX B

CONTROLLER CODE

In these appendix only the main modifications made on the original code developed in [2] have been reported

```
/*****************************************************************************
 * ControlRoutines.c
                     *
 *****************************************************************************/

void ReducedControlFiltering(inv_num inverter)
{
      Iout_filter.f_input    = AnalogIn.Iphase_W2;
      Vdc_filter.f_input     = AnalogIn.Vdc1;

      lpf_func(& Iout_filter);
      lpf_func(& Vdc_filter);

    }

void ReducedControlTask(inv_num inverter)
{
    if(Vdc_filter.f_output >= 60)
    {
        duty_U_reduced = 1;
    }
    else
    {
```

```
            reduced_pi.ref  = (Vdc_filter.f_output)*KV;

            reduced_pi.y    = Iout_filter.f_output;

            pi_std(&reduced_pi);
            duty_U_reduced=reduced_pi.u;

        }
    }

void ReducedControlDutyUpdate(inv_num inverter)
{
    PhaseU_DutyUpdate(inverter,duty_U_reduced);
    PhaseV_DutyUpdate(inverter,0);
    PhaseW_DutyUpdate(inverter,0);
}

void ReducedControlInit(){
    Vdc_filter.Ts   = TS_FILTER;
    Vdc_filter.pole = POLE_FILTER;
    Vdc_filter.f_input = 0;

    lpf_init(&Vdc_filter);

    Iout_filter.Ts      = TS_FILTER;
    Iout_filter.pole    =POLE_FILTER;
    Iout_filter.f_input = 0;
    lpf_init(& Iout_filter);

        duty_filter.Ts      = TS_FILTER;
        duty_filter.pole    =POLE_FILTER;
        duty_filter.f_input = 0;
        lpf_init(& duty_filter);

    reduced_pi.kc       = KC_RED;
    reduced_pi.Ts_Ti_kc = TS_TI_KC_RED;
    reduced_pi.ka_kc    = 0;
```

```
    reduced_pi.AW_low   = 0;
    reduced_pi.AW_up    = 1;

    duty_U_reduced          = 0.0;
    duty_U_reduced_Oloop    = 0.0;
}

/*********************************************************************************
 * ISR.c                                                             *
 *********************************************************************************/

 /* ePWM4 event-trigger interrupt -------------------------------------------- */
void epwm4_int_isr(void)
{
    if(sys_ctrl[INVERTER2].Int_ctrl_en){
            ReducedControlFiltering(INVERTER2);
            ReducedControlTask(INVERTER2);
          //  PhaseU_DutyUpdate(INVERTER2,duty_U_reduced_Oloop);
            ReducedControlDutyUpdate(INVERTER2);
        }
}

/*********************************************************************************
 * Main.c                                                                        *
 *********************************************************************************/

void main(void)
{ ...
   #else
    ePWM_ChInit(EPWM1, SWITCHING_FREQ, 0, MODE_UPDOWN|MODE_SYNCHOUT|MODE_INT, NOTZ, DEADTIME_NS);
    ePWM_ChInit(EPWM2, SWITCHING_FREQ, 0, MODE_UPDOWN|MODE_SOCA, NOTZ, DEADTIME_NS);
    ePWM_ChInit(EPWM3, SWITCHING_FREQ, 0, MODE_UPDOWN, NOTZ, DEADTIME_NS);
```

```
    ePWM_ChInit(EPWM4, SWITCHING_FREQ_RED, 0, MODE_UPDOWN|MODE_SYNCHOUT|MODE_INT,
        NOTZ, DEADTIME_NS);
    ePWM_ChInit(EPWM5, SWITCHING_FREQ, 0, MODE_UPDOWN, NOTZ, DEADTIME_NS);
    ePWM_ChInit(EPWM6, SWITCHING_FREQ, 0, MODE_UPDOWN, NOTZ, DEADTIME_NS);
  #endif

...
}
```